**İSTANBUL TECHNICAL UNIVERSITY ★ INSTITUTE OF SCIENCE AND TECHNOLOGY**

# CONTROLLED BIOMINERALIZATION TOWARDS TISSUE ENGINEERING USING GENETICALLY ENGINEERED HYDROXYAPATITE BINDING PEPTIDES

**M.Sc. Thesis by**

**Mustafa GUNGORMUS, B.Sc.**

**Department :** **Advanced Technologies in Science and Technology**

**Programme:** **Molecular Biology – Genetics and Biotechnology**

**JUNE 2006**

**İSTANBUL TECHNICAL UNIVERSITY ★ INSTITUTE OF SCIENCE AND TECHNOLOGY**

# CONTROLLED BIOMINERALIZATION TOWARDS TISSUE ENGINEERING USING GENETICALLY ENGINEERED HYDROXYAPATITE BINDING PEPTIDES

**M.Sc THESIS by**
**Mustafa GÜNGÖRMÜŞ, B.Sc.**
**(521031213)**

**Date of submission : 8 May 2006**
**Date of defence examination: 14 June 2006**

**Supervisor (Chairman):** **Assoc. Prof. Candan TAMERLER (İ.T.Ü.)**

**Prof. Dr. Mehmet SARIKAYA (U.W.)**

**Members of the Examining Committee** **Prof.Dr. Fikrettin ŞAHİN (Y.Ü.)**

**Assoc. Prof. Hakan BERMEK (İ.T.Ü.)**

**Assoc. Prof. Ayten Yazgan KARATAŞ (İ.T.Ü.)**

**JUNE 2006**

**İSTANBUL TEKNİK ÜNİVERSİTESİ ★ FEN BİLİMLERİ ENSTİTÜSÜ**

# GENETİK MÜHENDİSLİĞİ İLE ELDE EDİLEN, HİDROKSİAPATİTE BAĞLANAN PEPTİDLER İLE DOKU MÜHENDİSLİĞİNE YÖNELIK KONTROLLÜ BİYOMİNERALİZASYON

**YÜKSEK LİSANS TEZİ**

**Mustafa GÜNGÖRMÜŞ, B.Sc.**
**(521031213)**

**Tezin Enstitüye Verildiği Tarih: 8 Mayis 2006**
**Tezin Savunulduğu Tarih: 14 Haziran 2006**

| | |
|---|---|
| **Tez Danışmanları:** | **Doç. Dr. Candan TAMERLER (İ.T.Ü.)** |
| | **Prof. Dr. Mehmet SARIKAYA (U.W.)** |
| **Diğer Jüri Üyeleri** | **Prof. Dr. Fikrettin ŞAHİN (Y.Ü.)** |
| | **Doç. Dr. Hakan BERMEK (I.T.Ü. )** |
| | **Doç. Dr. Ayten Yazgan KARATAŞ (I.T.Ü.)** |

**HAZİRAN 2006**

**ACKNOWLEDGMENT**

I would like to thank to Associate Professor Candan Tamerler Behar and Professor Mehmet Sarikaya, my advisors, for their valuable guidance, endless support and continued advices.

I would also like to thank to Professor Mustafa Urgen and Associate Professor Gultekin Goller for providing and characterizing the hydroxyapatite powder substrate, Hilal Yazici, Semih Karabulut and Senem Donatan for their help with the phage display protocols, Doctor Hanson Fong for mineral characterization, sharing his ideas throughout the whole research and getting me acquainted with materials science, Doctor Ersin Emre Oren for sequence similarity analyses and sharing his ideas about phage binding characterization, Doctor Marketa Hnilova for her help with ELISA protocols.

Many thanks to my laboratory and room mates, Turgay Kacar and Urartu Ozgur Safak Seker, for their help with the laboratory maintenance and making this research more enjoyable with their moral support.

Special thanks to Sibel Cetinel not only for her help with phage display and DNA sequencing protocols, but also for giving her endless support and love, over different continents, at my most desperate times.

I am also greatly indebted to my family, my father Dursun Gungormus and my mother Fadime Gungormus. They have encouraged me for doing scientific research and never left me without their support. Without them, I wouldn't be able to write this acknowledgment.

I would like to thank to the funding agencies for making this study possible. This study was supported by United States Army Research Office (U.S. A.R.O.) through "Defense University Research Initiative in Nanotechnology" (DURINT) project, Turkish State Planning Organization (D.P.T.) through "Development of nanostructured materials and systems via biomimetics" project and Turkish State Planning Organization (D.P.T.) supported Molecular Biology-Genetics and Biotechnology Program at Istanbul Technical University (I.T.U.) as part of Advanced Technologies in Engineering Program.

JUNE, 2006 Mustafa GÜNGÖRMÜŞ

**TABLE OF CONTENTS**

**ABBREVIATIONS**

**AP** : Alkaline Phosphatase
**BGP** : Bone Gla Protein
**bp** : Base Pair
**BMP** : Bone Morphogenic Protein
**BSA** : Bovine Serum Albumin
**BSP** : Bone Sialoprotein
**DMF** : Dimethylformamide
**DNA** : Deoxyribonucleic Acid
**EB** : Elution Buffer
**ECM** : Extra Cellular Matrix
**EDTA** : Ethylenediaminetetraacetic Acid
**FITC** : Fluorescein IsoThioCyanate
**FM** : Fluorescence Microscopy
**GEPI** : Genetically Engineered Polypeptides for Inorganics
**HA** : Hydroxyapatite
**HABP** : Hydroxyapatite Binding Peptide
**HRP** : Horse Raddish Peroxidase
**IgG** : Immunoglobulin Gamma
**IPTG** : Isopropyl-β-D- Thiogalactopyranosi
**LB- broth** : Luria Bertani broth
**MGP** : Matrix Gla Protein
**MLB** : M13 Lysis Buffer
**MP** : M13 Precipated Buffer
**mRNA** : Messenger Ribonucleic Acid
**NMR** : Nuclear Magnetic Resonance
**OCN** : Osteocalcin
**OD** : Optical Density
**OPN** : Osteopontin
**PBS** : Phosphate Buffer Saline
**PFU** : Plaque Forming Unit
**PCR** : Polymerase Chain Reaction
**PEG-8000** : Poly-ethylene Glycol-8000
**RF** : Replicative Form
**SEM** : Scanning Electron Microscope
**SPARC** : Secreted Protein Acidic and Rich in Cysteine
**ssDNA** : Single Stranded Deoxyribonucleic Acid
**TBE** : Tris-Borat -EDTA
**TEM** : Transmission Electron Microscope
**XRD** : X-Ray Diffraction

**LIST OF SYMBOLS**

| | |
|---|---|
| **A** | : Alanine |
| **C** | : Cysteine |
| **D** | : Aspartic Acid |
| **$dH_2O$** | : Distilled water |
| **E** | : Glutamic Acid |
| **F** | : Phenylalanine |
| **G** | : Glycine |
| **H** | : Histidine |
| **I** | : Isoleucine |
| **K** | : Lysine |
| **kb** | : Kilobase |
| **L** | : Leucine |
| ***LacZ*** | : $\alpha$-galactosidase |
| **M** | : Methionine |
| **N** | : Apsparagine |
| **Na-Ac** | : Sodium acetate |
| **P** | : Proline |
| **PC** | : Potassium Phosphate-Sodium Carbonate buffer |
| **R** | : Arginine |
| **rpm** | : Revolutions Per Minute |
| **S** | : Serine |
| **T** | : Threonine |
| **TMP** | : 3,3',5,5' tetramethylbenzidine |
| **Tris base** | : Hydroxymethyl aminomethane |
| **Q** | : Glutamine |
| **V** | : Valine |
| **W** | : Tryptophan |
| **X-Gal** | : 5-Bromo-4-chloro-3-indolyl-D-galactoside |
| **Y** | : Tyrosine |

## LIST OF TABLES

**LIST OF FIGURES**

**CONTROLLED BIOMINERALIZATION TOWARDS TISSUE ENGINEERING USING GENTICALLY ENGINEERED HYDROXYAPATITE BINDING PEPTIDES**

## SUMMARY

Hydroxyapatite is the principal mineral of mammalian hard tissues, such as bone and teeth. Hydroxyapatite particles are found in various shapes and sizes in different tissues providing the specific functional properties of the tissues. Many proteins in bone and dental matrices are involved in the formation of the hydroxyapatite crystallites and their growth into myriad different nano and micro-architectures. These proteins affect hydroxyapatite formation at different times during the tissue generation and spatial locations in the tissue leading to the differences in the molecular composition, structure and self-assembly properties of hydroxyapatite.

Because of the enormous number of large proteins involved in the tissue generation and the current problems associated with the difficulties of quantifying their spatial and temporal distribution, we launched, first, to select genetically engineered polypeptides that have specific affinity to HA, and then investigate how hydroxyapatite binding peptides affect HA formation. We have combinatorially selected hydroxyapatite binding peptides via a commercial M13 C7C library. Binding characterization of the peptides was done via fluorescence microscopy and ELISA. The strongest binding clone, MG-49 and a weak binding clone, MG-63, were selected and the peptide sequence they display was commercially synthesized to study their effects in an AP mediated *in vitro* mineralization system. We observed that MG-49 inhibits nucleation of octacalcium phosphate, a precursor of hydroxyapatite, while it promotes the crystal growth compared to control and weak binding peptides. Kinetic analysis showed that MG-49 peptide shows its effect on crsytal morphology by controlling the reaction kinetics.

Combinatorially selected HA binding peptides may also find use in several different fields, such as bioinformatics, medical biomaterials and drug delivery applications in addition to hard tissue engineering.

## GENETİK MÜHENDİSLİĞİ İLE ELDE EDİLEN, HİDROKSİAPATİTE BAĞLANAN PEPTİDLER İLE DOKU MÜHENDİSLİĞİNE YÖNELIK KONTROLLÜ BİYOMİNERALİZASYON


## ÖZET

Hidroksiapatit, kemik ve diş gibi memeli sert dokularının birincil mineralidir. Hidroksiapatit parçacıkları vücutta farklı boyutlarda ve şekillerde bulunabilir. Bu farklı şekil ve boyutlar dokuların özgün işlevsel özelliklerini belirler. Diş ve kemik dokularında hidroksiapatit oluşumunda ve farklı mikro ve nano mimariler oluşturmasında rol alan birçok protein bulunur. Bu proteinler hidroksiapatit oluşumunu doku gelişimi sırasında farklı yerlerde ve zamanlarda etkileyerek farklı moleküler bileşimlerde ve yapılarda hidroksiapatit oluşumunu sağlarlar.

Doku gelişiminde rol alan proteinlerin sayısının çok fazla olmasından ve proteinlerin zamansal ve mekansal dağılımlarının belirlenmesindeki zorluklardan dolayı, bu çalışmada ilk önce genetik mühendisliği ile hidroksiapatite özgün olarak bağlanan peptidler seçip, daha sonra bu peptidlerin hidroksiapatit oluşumunu nasıl etkilediğini inceleme yolunu seçtik. Hidroksiapatite özgün olarak bağlanan peptidler ticari bir kütüphane olan M13 C7C kütüphanesi aracılığı ile seçildi. Peptidlerin bağlanma özellikleri flüoresan mikroskopisi ve ELISA yöntemleri ile karakterize edildi. Karakterizasyon sonucunda en kuvvetli bağlanan klon, MG-49, ve zayıf bağlanan bır klon, MG-63, seçilerek mineralizasyon çalışmaları için peptid dizileri ticari olarak sentezlendi. Mineralizasyon çalışmaları için Alkalin Fosfataz aracılıklı bir mineralizasyon sistemi kullanıldı. Mineralizasyon çalışmaları MG-49 peptidinin, hidroksiapatitin bir öncülü olan oktakalsiyum fosfat nükleasyonunu baskıladığı fakat kristallerin büyümesini tetiklediğini gösterdi. Tepkime kinetiği analizleri MG-49 peptidinin kristallerin morfolojilerinde oluşturduğu etkisini tepkime kinetiğini kontrol ederek gösterdiğini ortaya koydu.

Kombinasyonel olarak seçilen hidroksiapatite bağlanan peptidler, malzemeye yüksek özgünlük, seçicilik ve bağlanma özellikleri gösterebildiklerinden yalnızca sert doku mühendisliğinde degil, biyo-bilişim, biyo-uyumlu yüzeylerin, biyo-malzemelerin oluşturulmasında ve kontrollü ilaç salınımı gibi farklı alanlarda da kullanılabilir.

# 1. INTRODUCTION AND BACKGROUND

## 1.1. The Importance of Proteins in Biomineralization

The regulated formation of inorganic minerals in living systems is called biomineralization. The ability to deposit minerals in living organisms serves for various purposes. It is most important for the formation and proper shaping of hard parts, such as bone, teeth and seashells. The mineral deposits are also used by organisms for maintaining homeostatic cellular levels of inorganic ions. For plants, mineral crystals such as calcium oxalate crystals can also be used for defense. A great variety of organisms posses the ability to deposit minerals. For example, magnetotactic bacteria deposit magnetite ($Fe_3O_4$) or greigite ($Fe_3S_4$) crystals enclosed in organic sheaths, Blakemore (1975), mollusks form calcite crystals in their shells, Weiner *et al*. (1976), diatoms form a highly silicified cell wall, Reimann and Lewin (1964), some cactus plants form calcium oxalate crystals, Gibson and Horak (1978) and vertebrates generate apatite crystals, found in bone and teeth (Lowenstam and Weiner, 1989). (Figure 1.1.)

The main difference between biogenic and synthetic mineral deposits is that the mineralization process in living organisms is strictly regulated by a specific set of biomolecules, typically by proteins, while only a limited control can be established over the properties of synthetic materials. Proteins (also proteolipids and proteoglycans), regulate the balance between crystal saturation and precipitation in solution, inhibition or promotion of nucleation and growth of mineral crystals and the overall structure and the assembly of the crystal (Lowenstam and Weiner, 1989)

The proteins regulating the biomineralization processes are studied generally under two main classes; acidic proteins and framework proteins. Acidic proteins are named as such because their function is intimately connected to their acidic nature and abundance of polar side chains that are negatively charged at neutral pH. Typically, acidic proteins are rich in aspartate, glutamate, phosphorylated serine, tyrosine, and threonine. In vertebrates, these acidic proteins are found in bone, salivary fluids, and the urinary tract and bladder (Long *et al*, 1998). These proteins may also be covalently bonded to polysaccharides, which are rich in carboxylate, to

form acidic proteoglycans. The acidic proteins are intimately associated with the mineral and regulate mineral formation. (Long *et al*, 1998)

The second type of proteins involved in biomineralization is the framework proteins. The function of framework proteins is true to their name. They serve as scaffolds for mineral deposits, and they tend to be insoluble, relatively hydrophobic and are typically cross-linked. Collagen, found in bone tissue, is an excellent example of a framework protein, because its long, α-helix shape, with three interwoven strands, is very robust and provides shape to the crystalline tissue (Lowenstam and Weiner, 1989).

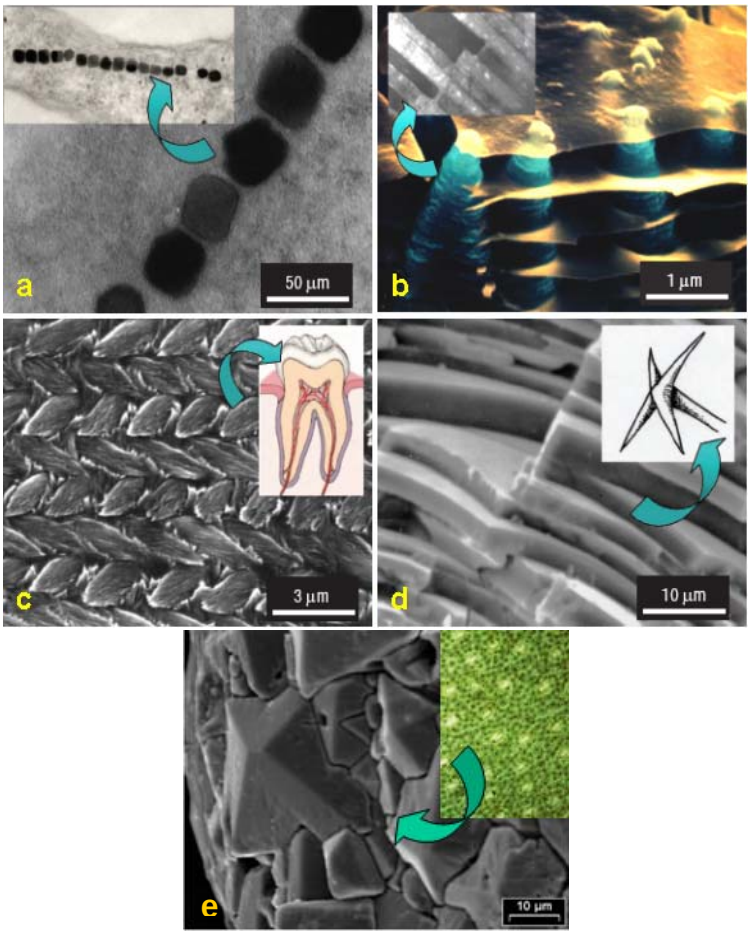


**Figure1.1:** Examples of biogenic minerals: **a)** SEM image of single crystalline, single domained and crystallographically aligned magnetite nanoparticles formed by A. magnetotacticum. (Inset: TEM image) **b)** SEM image of a growth edge of abalone (Haliotis rufescens) displaying aragonite platelets (blue) separated by organic films (orange) that eventually becomes nacre (inset: TEM) image) **c)** SEM image of highly ordered hydroxyapatite crystallites in mouse enamel (inset: schematic cross-section of a human tooth) **d)** SEM image of silica layers of the sponge spicule of Rosell. (Schematic illustration of the cross-shaped apex) (a-d: Sarikaya *et al*, 2003) **(e)** SEM image of the calcium oxalate particles produced by the Cactus senilis (inset: optical microscopy image of the Cactus senilis epidermis. Black features are the calcium oxalate crystals. (Gibson and Horak, 1978)

### 1.1.1. Hydroxyapatite: Formation and Proteins

Hydroxyapatite (HA) is a naturally occurring form of calcium apatite with the formula $Ca_5(PO_4)_3(OH)$, but is usually written $Ca_{10}(PO_4)_6(OH)_2$ to denote that the crystal unit cell comprises two molecules. The hydroxyl ion in the structure can be substituted by fluoride, chloride or carbonate.

HA is the principal mineral of mammalian hard tissues, such as bone and teeth. (Lowenstam and Weiner, 1989) However, hydroxyapatite particles are found in various shapes and sizes in different tissues providing the specific functional properties of the tissues. For example, mammalian tooth's inorganic part is composed of three different layers, from top to bottom, enamel, dentin and cementum (Lowenstam and Weiner, 1989) (Figure 1.2.). The main constitution of these layers is HA. However, each of these tissues possesses unique mechanical properties originating from different organizations of HA crystals. Highly ordered HA nano-rods in the enamel provide the extraordinary hardness of the tissue (Fong *et al*, 2003). Tubular organization of the dentin provides the teeth the ability to flex and absorb tremendous functional loads without fracturing (Kinney *et al*, 2003). The plate like structure of cementum provides the softness of the tissue allowing the attachment of the periodontal ligaments (He *et al*, 2003).

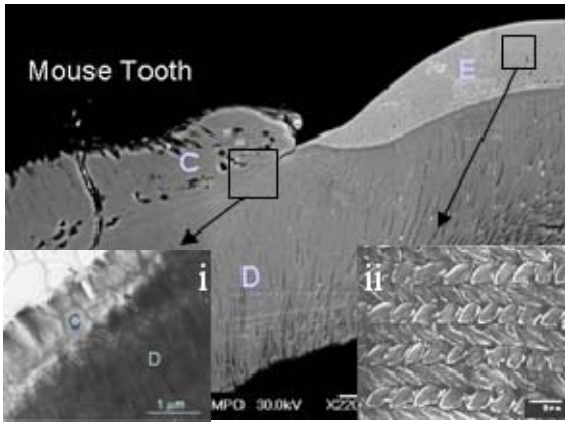


**Figure 1.2:** SEM image of cross-section of a mouse incisor tooth. Morphological differences are clearly seen between (E) Enamel, (C) Cementum and (D) Dentin, (inset: i; high magnification of the dentin-cementum junction area. ii; high magnification of enamel crystals) (Fong *et al*, 2003)

From this standpoint, *in vitro* fabrication of hydroxyapatite with controlled size, shape and properties has been a significant goal in the filed of restorative and regenerative biomaterials. This challenge has been the focus of intensive research for many years. There is an enormous amount of literature dealing with the fabrication pathways of HA. Synthetic HA particles have been produced by a variety of routes

including hydrothermal processing, Mengeot *et al*. (1973), wet chemical precipitation, Lopez-Macipe *et al*. (1998), Afshar *et al*. (2003), sol–gel, Layrolle *et al*., (1998), Deptula *et al.* (1993), solid state reactions, Verbeerck *et al*. (1995). Other HA synthesis methods, such as microwave irradiation, Lerner *et al*. (1991), spray pyrolysis, Luo *et al*. (1995), and mechano-chemical treatment, Rhee *et al*. (2002) have also been reported. However, biomimetic approach for the synthesis of HA has gained an increasing attention over the last few years since, in contrast to the methods listed above; the synthesis is carried out at 37$^{o}$C, neutral pH and in ionic environments similar to those of human body with the biomimetic approach. (Tanahashi *et al*., 1994. Schwarz *et al*., 1998. Feng *et al*., 2005). Therefore, this synthesis route shares many similar properties with the biological synthesis of HA in vertebrate body.

The mineralization process of vertebrate hard tissues include the synthesis of an extra cellular matrix (ECM) by ECM forming cells (ameloblasts, osteoblasts, dentinoblasts, etc.) and deposition of minerals within the ECM. The nucleation-growth kinetics and the morphology of HA are regulated by a specific set of biomolecules, called ECM proteins. (Lowenstam and Weiner, 1989). ECM proteins are studied under two classes; “collagenous ECM proteins” and “non-collagenous ECM proteins” (Lowenstam and Weiner, 1989).

Collagen is the most abundant organic component of the bone and dentin (50 - 90% of protein content). It is also the most abundant protein in human body. Collagen in bone and dentin are mainly Type I collagen. Type I collagen in bone is produced from the same gene as that in soft tissues (Rich *et al,* 1961). Therefore, Type I collagen in bone is essentially the same molecule as that in non-calcified tissue. The difference between bone collagen and non-calcified tissue collagen arise from the posttranslational modifications. These modifications include hydroxylation of lysine residues, glycosylation of hydroxylysine, and phosphorylation, and are believed to play an integral role in collagen mineralization (Kao *et al*, 1965). From the viewpoint of hydroxylation, for example, the extent of hydroxylation of lysine residues is much higher in bone collagen than in non-calcified tissue. The extent and site of the hydroxylation governs cross-linking patterns, hence, packing of collagen molecules (Figure 1.3.). It is noteworthy that the average gap between collagen molecules in tendons is smaller than the diameter of phosphate ion, although that in bone is larger than that of phosphate ion which enables the phosphate ions migrate into collagen fibrils (Rich *et al,* 1961).

During the mineralization process, apatite crystals grow preferentially lengthwise in the direction of the long axis of collagen and in width along channels or grooves that are formed by adjacent hole zones of collagen. Collagen fibers overlap adjacent fibers as they repeat every 680 Å. Hole zones are the areas of low-density bone collagen and overlap zones are areas of very high-density collagen. Hydroxyapatite crystals are arranged in layers within each fiber, resembling overlapping bricks. These combined properties, plus the degree of bonding between the collagen fibers and the crystals, provide a robust structure that has both extreme tensile and compression strength, making the bone, on a weight basis, stronger than concrete. However, numerous studies indicate that collagen is not a direct nucleator of apatite deposition. Rather, collagen provides a template for mineral deposition which may be initiated by associated non-collagenous proteins (Kao *et al*, 1965).

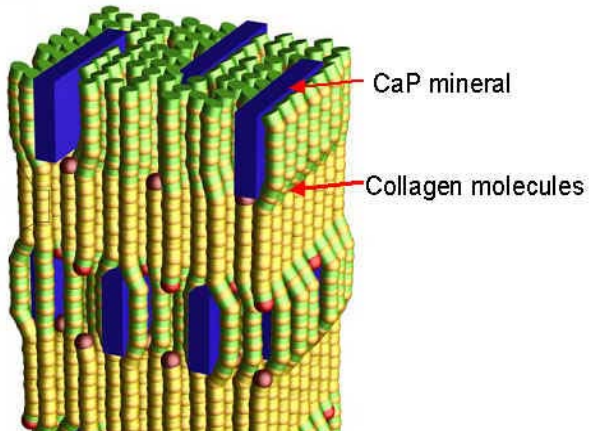


**Figure 1.3:** Schematic representation of the molecular arrangement of collagen and hydroxyapatite crystals in compact bone. (Kinney *et al*, 2003)

Non-collagenous proteins are mostly tissue specific and compose of a small portion of the organic part of the hard tissues. (*Lowenstam, H.A. 1989*). A list of major and best characterized non-collagenous proteins influencing mineral formation during bone and teeth development are listed in Table 1.1.

**Table 1.1:** List of major non-collagenous proteins influencing HA formation during bone and teeth development. Symbols (f) and (i) indicate free and immobilized proteins, respectively.

| Protein | HA Formation | Remarks |
|---|---|---|
| Osteopontin | Inhibits mineralization (Hunter *et al,* 1996) | Promotes cell attachment (McKee *et al*, 1996) |
| Bone Sialoprotein II | Promotes nucleation (Hunter *et al,* 1993) | Binds to HA and collagen<br>Promotes osteoblast differantioation (Zhou *et al*, 1995) |
| Bone Morphogenic Proteins | Embryonic patterning (Chen *et al*, 2004) | Growth Factors (Chen *et al*, 2004) |
| Matrix GLA protein | Inhibits mineralization (Luo *et al*, 1997) | Binds to HA and $Ca^{+2}$ (Price *et al*, 1985) |
| Osteocalcin ( f ) | Inhibits mineralization (Price *et al*, 1981)<br>Inhibits seeded growth (Romberg *et al*, 1986) | Inhibits osteoblast activity (Ducy *et al*, 1996)<br>Binds to HA, but not to ACP (Price *et al*, 1976) |
| Osteocalcin ( i ) | Promotes mineralization (Doi *et al*, 1993) | Binds to HA (Fujisawa *et al*, 1991) and collagen (Fujisawa *et al*, 1992) |
| Osteonectin ( f ) | Inhibits mineralization (Doi *et al*, 1992) | Binds to HA and collagen (Romberg *et al*, 1985) |
| Osteonectin ( i ) | Promotes mineralization (Termine *et al*, 1981) | Links HA to collagen (Termine *et al*, 1981) |
| Dentin phosphoprolyn ( f ) | Inhibits mineralization at high concentration (Doi *et al*, 1992) | Binds to collagen (Veis, 1993)<br>Binds to Ca and $PO_4$ ions (Massh, 1989)<br>Binds to HA (Fujisawa *et al*, 1991) |
| Dentin phosphoprolyn ( i ) | Promotes formation mineralization (Doi *et al*, 1993) | |
| Amelogenin | Aligns crystals into parallel arrays (Beniasha *et al*, 2005)<br>Modulates cell attachment (Hoang *et al*, 2002) | Binds to HA (Ryu *et al*, 1999) |
| Statherin | Inhibits mineralization (Moreno *et al*, 1979) | Binds to mineral (Schlesinger *et al*, 1977) |
| Enamelin | Inhibits formation (Romberg *et al*, 1986) | Binds to mineral (Yanagisawa *et al*, 1981) |

Bone sialoprotein is one of the most important extra cellular matrix proteins in bone. It has been showed that BSP message is up-regulated up to over 140 fold in osteoblasts as the cultured cells undergo a massive wave of mineralization, and that it can promote *de novo* nucleation of apatite crystals *in vitro* (Ibaraki *et al.,* 1992). The promotional effects of bone sialoprotein on hydroxyapatite formation are due to the polyglutamicacid rich region at the N-terminus of the protein. The major cell attachment site (RGD) is near the C-terminus in a coil structure, surrounded by sulphated tyrosines and separated from the HA-binding region by sites of extensive N- and O- linked glycosylation (Ganss *et al.*, 1999). (Figure 1.4.)

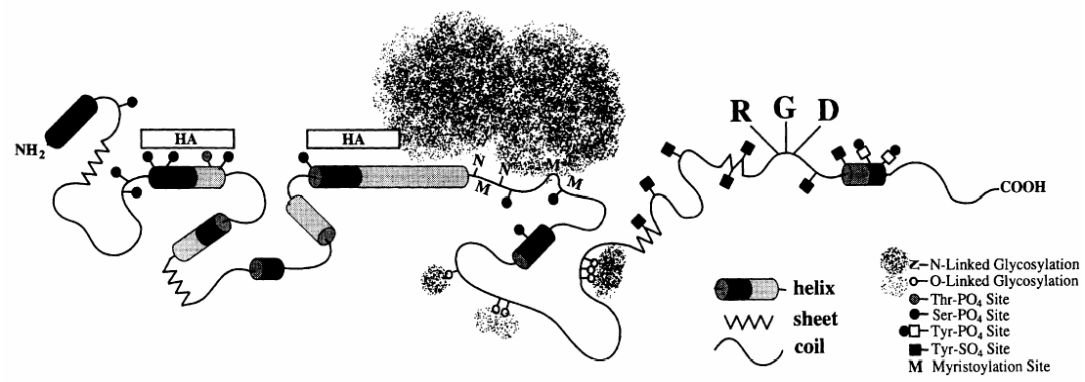


**Figure 1.4:** Schematic structure of Bone Sialoprotein (Ganss *et al*, 1999)

Matrix Gla protein (MGP) has been shown to have a hydroxyapatite binding domain (Price *et al.*, 1985). Studies on MGP-deficient mice have shown an increase in the ectopic calcification, which suggest that MGP is an inhibitor of spontaneous calcification in arteries and the epiphyseal growth plate (Luo *et al.*, 1997).

Osteocalcin, also known as bone Gla protein (BGP) is exclusively found in bone tissue, accounting for 10-20% of the non-collagenous protein content of the bone. Osteocalcin contains gamma-carboxyglutamic acid (Gla) and has affinity to calcium and hydroxyapatite Gamma-carboxyglutamic acid (Gla) residues (green), responsible for $Ca^{+2}$ binding are at positions 17, 21 and 24 and a disulphide bound is present between residues 23 and 29. (Hoang *et al.*, 2003) (Figure 1.5.). A number of studies have demonstrated the inhibitory effects of osteocalcin on hydroxyapatite formation when it is free in solution, Price *et al.* (1981) but promoter effects when immobilized, Doi *et al.* (1993), indicating that protein conformation is also important in the process of mineralization. In dentin, osteocalcin is a very minor constituent. Osteocalcin appears to be more involved in the regulation of bone turnover, particularly in the inhibition of hypercalcification.

Osteonectin, also known as secreted protein acidic and rich in cysteine (SPARC) or basement membrane protein BM-40 binds strongly to hydroxyapatite (Sage *et al*, 1989). It modulates attachment of the cells to the mineral with its affinity to other ECM proteins including collagen type I, III, V, VIII, Sage *et al.* (1989) and IV, Mayer *et al* (1991), thrombospondin, Clezardin *et al.* (1991) and PDGF-AB and PDGF-BB, Raines *et al.* (1992). Osteonectin also binds to and inhibits the spreading of endothelial and smooth muscle cells (Sage *et al.*, 1989).

Although less than 5% of enamel consists of protein, enamelins comprise 2% of all enamel protein. The *in vivo* role of enamelin on enamel formation is still not clear but the enamelin proteins appear to be concentrated in areas closely surrounding the enamel mineral crystal surfaces, implying an important role in enamel formation (Yanagisawa *et al.*, 1981).

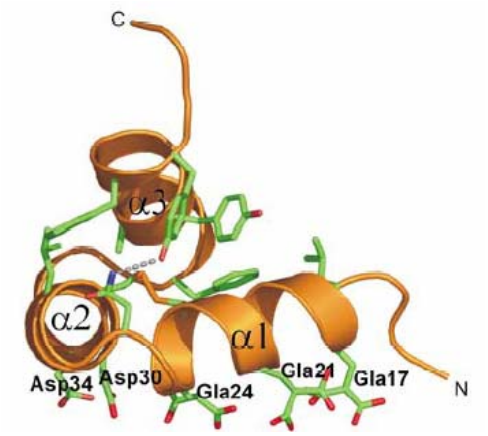


**Figure 1.5:** Simulation of the secondary structure of Osteocalcin. (Hoang *et al.*, 2003)

Osteopontin is a single chain acidic glycoprotein. Its N-terminus binds to HA crystals and farther down the peptide backbone is an RGD amino acid sequence that binds to a cell surface protein (Flores *et al.*, 1992, Gorski, 1991). This RGD sequence promotes the nucleation when bound to cell surface by locking the protein in a conformation that leaves certain crystal surfaces uninhibited (Gorski, 1991). (Figure 1.6.)

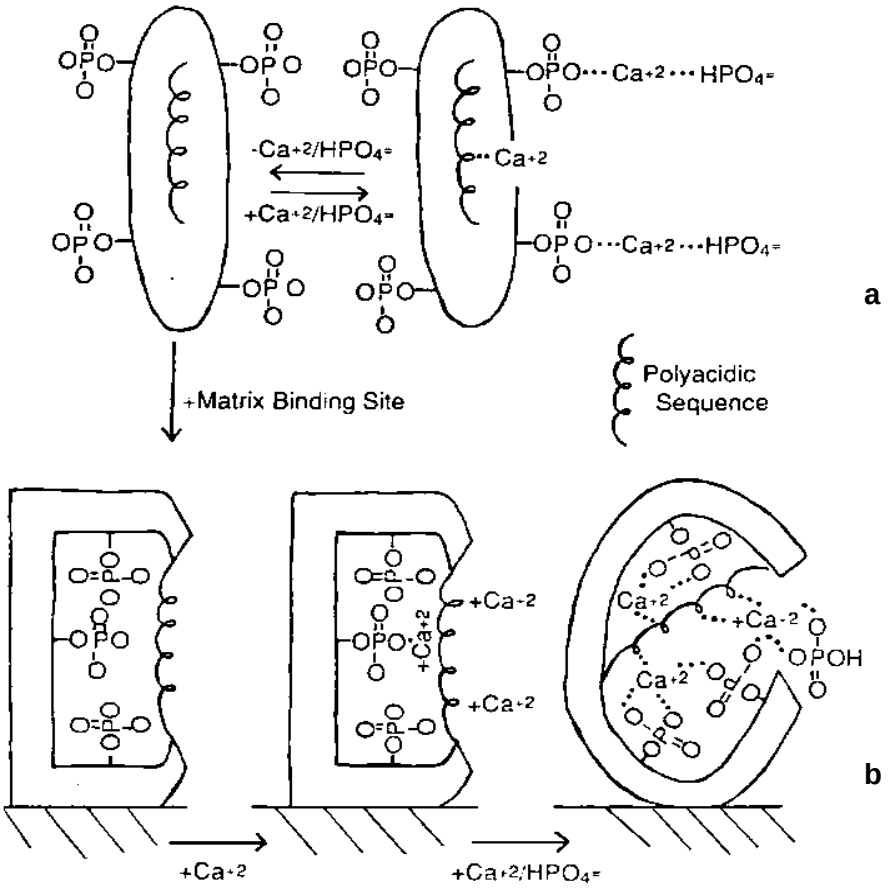


**Figure 1.6:** A proposed mechanism for osteopontin's ability to nucleate hydroxyapatite crystals and influence on the orientation of crystal growth when bound **(b)** versus inhibiting growth while in solution **(a)** (Gorski, 1991)

Dentin phosphophoryn is a dentin-specific protein and also the most abundant non-collagenous protein in dentin (Dimuzio and Veis, 1978). A histological study of dental tissues from Dentinogenesis Imperfecta type II (DGI-II) affected patients has shown that the affected tooth is very different in the DGI-II patient as compared with the normal dental tissue. In particular, the dentinal tubules in DGI-II are very irregular, which could be the result of perturbations in the process of dentin formation. The same study has shown a dramatic difference in the restriction length polymorhism patterns (RFLP) of Dentin phosphophoryn-2 gene between the affected and normal patients, indicating that indicated that dentin phosphophoryn might be a candidate gene in DGI-II. (Thotakura *et al*, 2000)

Statherin is one of the most studied and best understood proteins that influence HA formation. Statherin is a phosphoprotein found in human parotid and submandibular saliva and shows a high affinity to hydroxyapatite (Johnsson *et al.*, 1993). It has been showed that statherin prevents unwanted and potentially harmful mineralization in the oral cavity by functioning as the inhibitor of HA crystal nucleation and crystal growth (Johnsson *et al.*, 1993). Statherin has a pI of 4.2, and

it is negatively charged in biological conditions and all but one of the charged residues is present in N-terminus end of the polypeptide, illustrating the importance of the N-terminus for HA affinity (Schelsinger *et al*, 1977). Specifically, the aspartate, two phosposerines, and two glutamates located near the N-terminus are essential to statherin's binding affinity for HA crystals. Solution NMR studies have shown that Statherin is unstructured in aqueous solution, but it has been found that the N-terminal fragment adopts a helical conformation upon binding to hydroxyapatite (Shaw *et al*, 2000). (Figure 1.7.)

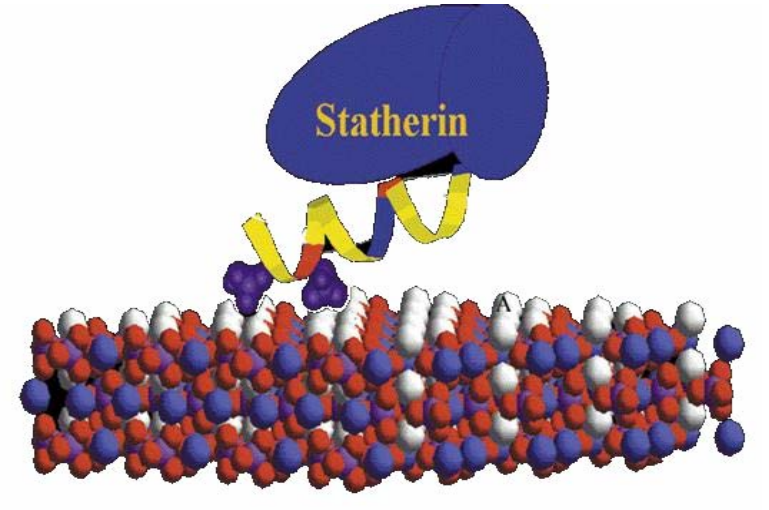


**Figure 1.7:** Schematic illustration showing statherin interacting with the 001 face of HA, with calcium ions in white and phosphoserines in purple. (Shaw *et al*, 2000).

Amelogenin is a gene-specific, low-molecular-weight protein found in tooth, comprising 90% of all enamel proteins. Although not completely understood, the function of amelogenin is believed to be in organizing enamel rods into parallel arrays during tooth development (Figure 1.8., 1.9) and regulating the initiation and growth of hydroxyapatite crystals during the mineralization of enamel (Ryu *et al*, 1999). Amelogenin is synthesized and secreted by ameloblast cells (Figure 1.8 - 1) and assemble into nano-sphere structures approximately 20 nm in diameter with an anionic surface (Figure 1.8 - 2). The nanospheres interact electrostatically with the elongating surfaces of the enamel crystallites, acting as 20nm spacers that prevent crystal-crystal fusions (Figure 1.8 - 3). Enzymes (Proteinase-1) eventually digest away the charged surface of the nanosphres, producing hydrophobic nanospheres that further assemble and stabilize the growing crystallites. Finally, other enzymes degrade the hydrophobic nanospheres, generating amelogenin fragments and other unidentified products, which are resorbed by the ameloblasts (Figure 1.8 - 4). As the amelogenin nanosphere protection is removed, crystallites thicken and eventually may fuse into mature enamel (Figure 1.8 - 5).

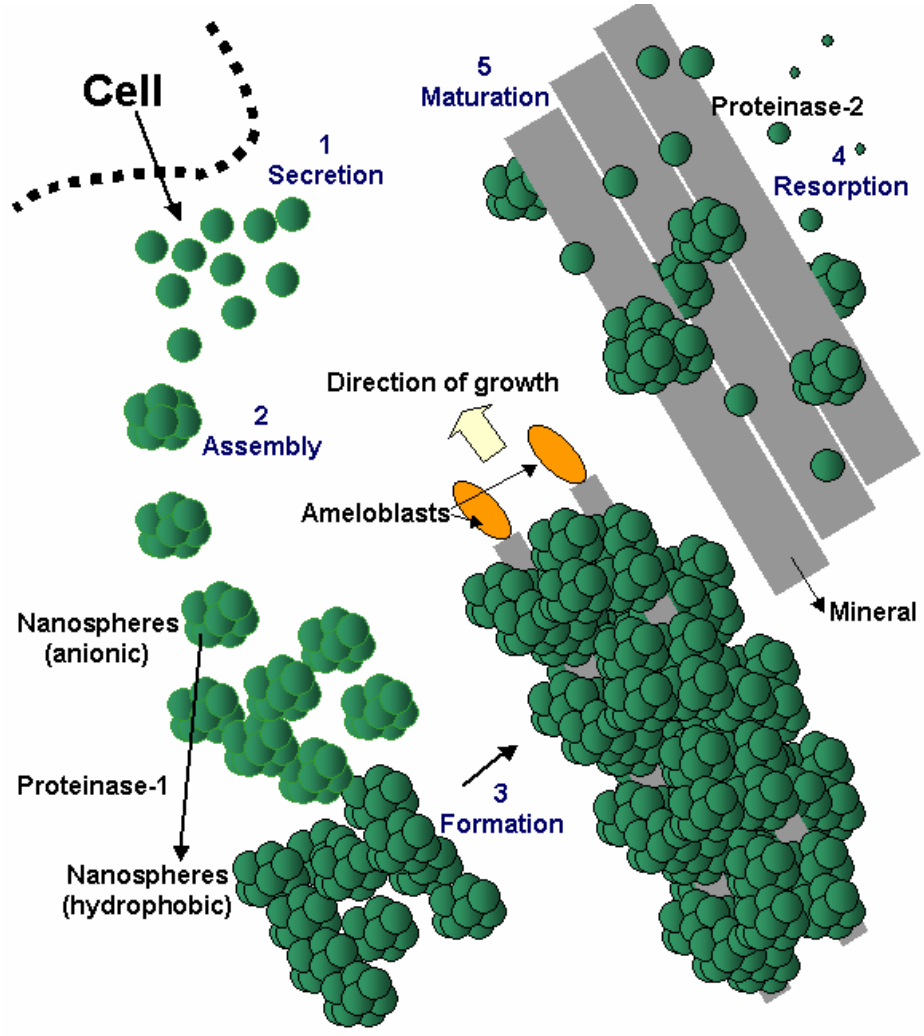


**Figure 1.8:** A hypothetical model for the role of amelogenin in enamel biomineralization (Reproduced from Fincham *et al.*, 1999)

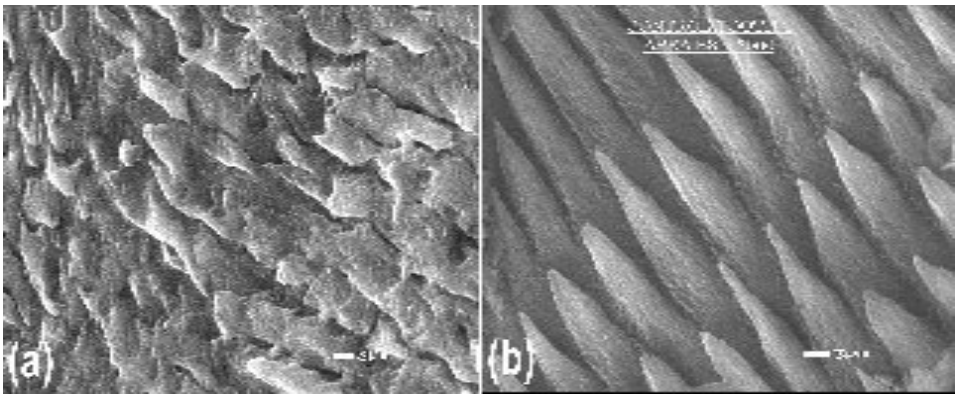


**Figure 1.9:** SEM image showing enamel architecture **(a)** in dysplastic tissue in amelogenesis imperfecta, which is a genetic disorder caused by incompetent amelogenin synthesis, compared with **(b)** a similar region in a normal tooth. Irregular arrangement of crystals causes loss of mechanical strength in the enamel (Ryu *et al.*, 1999).

### 1.2. Molecular Biomimetics and Applications

Biomimetics (also known as bionics, biognosis or biomimicry) is the application of methods and systems found in nature to the study, design and engineer materials. The biological world has long been a source of inspiration for engineering design. The popularity of designs that mimic natural systems is due, in large part, to advantages in performance. In the past, drawing ideas from nature was limited to macroscopic engineering problems (Ball, 2001. Vogel,1999). Advances in analytical techniques over the past several decades have opened the door to understanding the materials' structure and properties at the molecular level and have provided a better understanding of the potential of the nanotechnology (Ferry and Goodnick, 1997. Harris, 1999). However, the realization of the full potential of nanotechnological systems has so far been limited due to the difficulties in their synthesis and subsequent assembly into useful functional structures and devices. Even the most advanced conventional micro and nanotechnology processes have the limitations of large-scale synthesis of complex nano-scale architectures (Sarikaya *et al*., 2004). The product is so small in quantity and often not reproducible because of the nonspecific interactions, uncontrolled agglomeration, uncontrolled surface chemistry, and difficulties in multidimensional assembly for the widespread use (Harris, 1999). Biomaterials, on the other hand, are highly organized from the molecular to the nano- and macro scales, often in a hierarchical manner, with complex nano-architectures (Sakiyama-Elbert and Hubbell, 2001. Mayer and Sarikaya, 2002). Therefore, the transfer of technology between living organisms and synthetic constructs allows us to mimic natural structures at the micro and nano scales. This technology transfer is most desirable because evolutionary process' typically forces natural systems to become as highly optimized and efficient as possible. Also, biological materials are synthesized in aqueous environments under mild physiological conditions, such as neutral pH, room / body temperature, atmospheric pressure, while conventional engineering methods involve techniques like melting and solidification processes, thermo mechanical treatments, solution / vacuum deposition and growth processes requiring stringent conditions such as high heat and pressure and often producing toxic byproducts (DeGarmo *et al*, 1988).

In the process of synthesis of hard, as well as soft tissues in biological systems, proteins play a key role by both collecting and transporting raw materials, self- and co-assembling subunits into short- and long-range-ordered nuclei and substrates (Sarikaya and Aksay, 1995. Mann, 1996. Lowenstam and Weis, 1989). Whether in controlling tissue formation, biological functions or physical performance, proteins

are an indispensable part of biological structures and systems. Therefore, a simple conclusion is that the next-generation biomimetic engineering systems should include proteins in synthesis, assembly or function (Sarikaya, 1999, Seeman and Belcher, 2002, Ball, 2001) (Figure 1.10.)

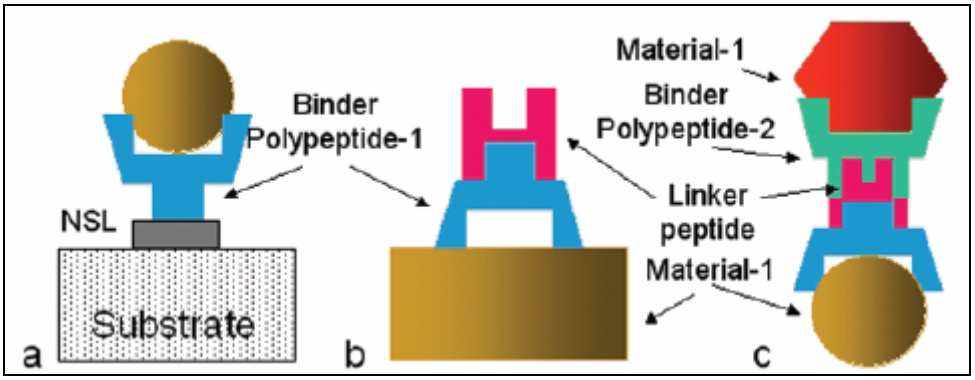


**Figure 1.10:** Potential uses of GEPI in engineering systems. **(a)** linkers for nanoparticle immobilization, **(b)** functional molecules that self-assemble on specific surfaces, **(c)** heterofunctional linkers involving two (or more) binding proteins adjoining several nanoinorganic units. (Sarikaya *et al.*, 2003).

### 1.3. Selection of Inorganic-binding Peptides

#### 1.3.1. Display Technologies

A limited number of natural proteins that bind to inorganic materials have been successfully identified and isolated up to date. One example of these proteins is the ice-binding protein found in many fish species, plants and insects. By binding to ice in the internal fluids of the organisms, these proteins control the particle size, morphology, or distribution of ice crystals preventing the freezing damage caused by the ice crystals (Liou *et al.*, 2000). Several approaches have been utilized in the search of inorganic-binding proteins to understand the inorganic-protein interactions with the intent to exploit this knowledge in producing biocompatible materials.

One approach used to obtain inorganic binding proteins is extracting and purifying proteins directly from hard tissues and cloning the genes coding them (Cariolou and Morse, 1988). This approach is a straightforward approach to obtain inorganic binding proteins but adverse consequences of this approach are that hard tissues contain a great number of proteins (Paine and Snead, 1996) and extraction and purification process' of the proteins may be extremely time consuming.

Another approach is designing inorganic-binding proteins by using theoretical molecular approach (Schonburn *et al.*, 2002). In this technique, the amino acid sequence and structure of the proteins are predicted by computational biology. This approach may be less expensive than other approaches however our little

knowledge about the number and structure of the proteins involved in the synthesis of biogenic materials makes theoretical design an impractical and time consuming approach.

Combinatorial biology, on the other hand, is an emerging field in design of inorganic binding proteins (Pelletier and Sidhu, 2001). In the combinatorial approach, a randomized pool of amino acid sequences is created and displayed on the surface of a host organism by genetic engineering. Then a target substrate is exposed to the randomized library. After removing the non-specific or weak binders with washing steps, specific and strong binders are recovered from the target substrate and sequenced. “Phage Display” and “Cell Surface Display” are two techniques widely used in vitro combinatorial biology techniques (Lee *et al.*, 2003. Smith and Petrenko, 1997). These techniques have been first developed to explore the interactions between organic molecules (Smith, 1985), however have been adapted to explore the organic - inorganic interactions, providing a tool for selection of inorganic binding peptides (Sarikaya, 1999. Mao *et al.*, 2003. Brown, 1992). Up to date, phage display has been successfully employed by several groups to identify peptides that are specific to gallium arsenide, Whaley *et al.* (2000), silica, Naik *et al.* (2002a), silver, Naik *et al.* (2002b), zinc sulfide, Lee *et al.* (2002), calcite, Li *et al.* (2002), cadmium sulfide, Mao *et al.* (2003), titanium, Sano *et al.* (2005) and carbon nanotubes, Wang *et al.* (2003). Cell surface display also has been applied to identify the iron oxide, gold (Brown, 1992), zinc oxide, zeolites and cuprous oxide, Nygaard *et al.* (2002), binding peptides.

### 1.3.2. Phage Display

Phage display has first been developed by G. Smith to explore the interactions between organic molecules (Smith, 1985). Phage display involves the expression of random amino acid sequences on coat proteins of the phage. Randomized DNA fragment encoding the random amino acid sequence is inserted to one of the permissive sites of the phage coat protein (Figure 1.13.), resulting in the phage particle to display the encoded peptide on the coat protein and contain its gene in the genome. This allows identifying the selected clones simply by DNA sequencing (Figure 2.4.).

Various vectors are used as vehicles for phage display. The first developed vehicle, filamentous bacteriophage M13 (Ff family), is the most widely used (Smith, 1985). This is due to ease of manipulating phage genome and obtaining high titers of phage ($10^{11\text{-}12}$ phages particles per milliliter). Besides these advantages, filamentous

phage vehicles have some drawbacks regarding to the size of the displayed peptide. The infection of the cell by the filamentous phage is a complex process involving the entry of the phage particle into the cell through the cell membrane. The phage g3p second N-terminal domain (N2) interacts with the F-pilus on the outside of the bacteria (Figure 1.12.a). After F-pilus retraction, the first N-terminal domain of g3p (N1) binds to the C-terminal domain of bacterial TolA (TolAIII) (Figure 1.12.b). The retracting pilus brings phage g3p domains in closer contact with TolA domains. As a consequence, the TolA can assume a more compact state of assembly, thus bringing the outer and inner membranes of the bacteria closer together (Figure 1.12.c). The phage g3p is inserted into the inner membrane, and the cap of the phage head is opened to allow phage DNA to enter the bacteria. (Figure 1.12.d) (Karlsson *et al*., 2003). Whereas these limitations interfere with the properties of desired protein to be expressed, phage λ, T7 or T4 can be preferred to display peptides with various sizes. Although there are some studies on λ, T7 or T4 phage-based display systems, they are not yet used in a routine way. (Hoess, 2002. Danner and Belasco 2001).

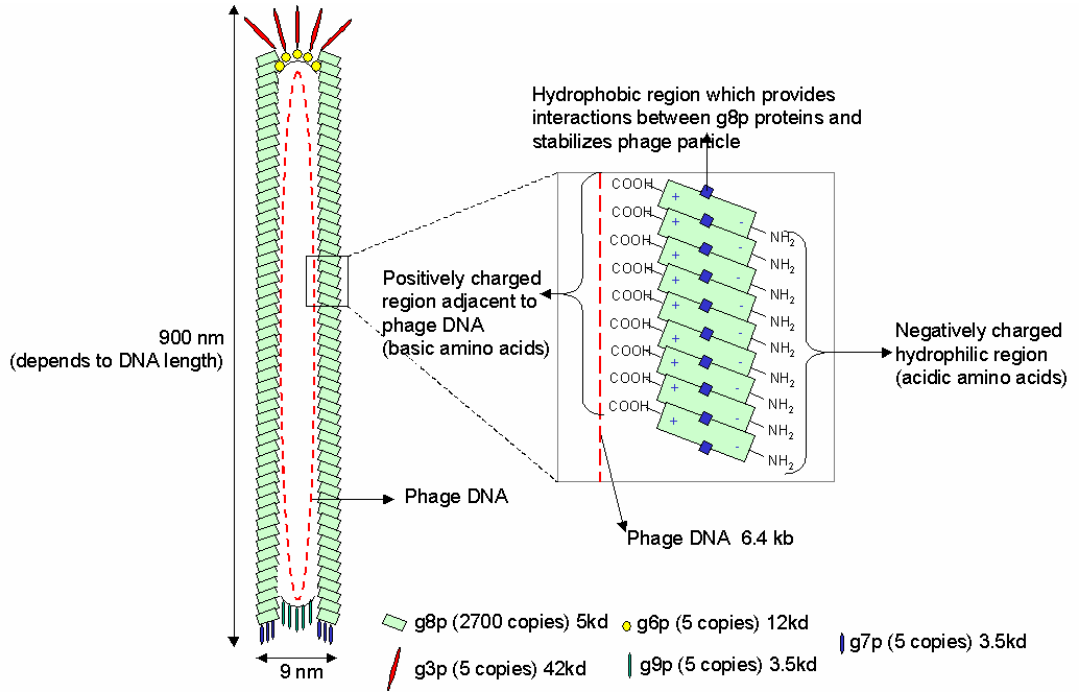


**Figure 1.11:** Schematic illustration of the structure of M13 bacteriophage (adapted from Smith and Petrenko, 1997)

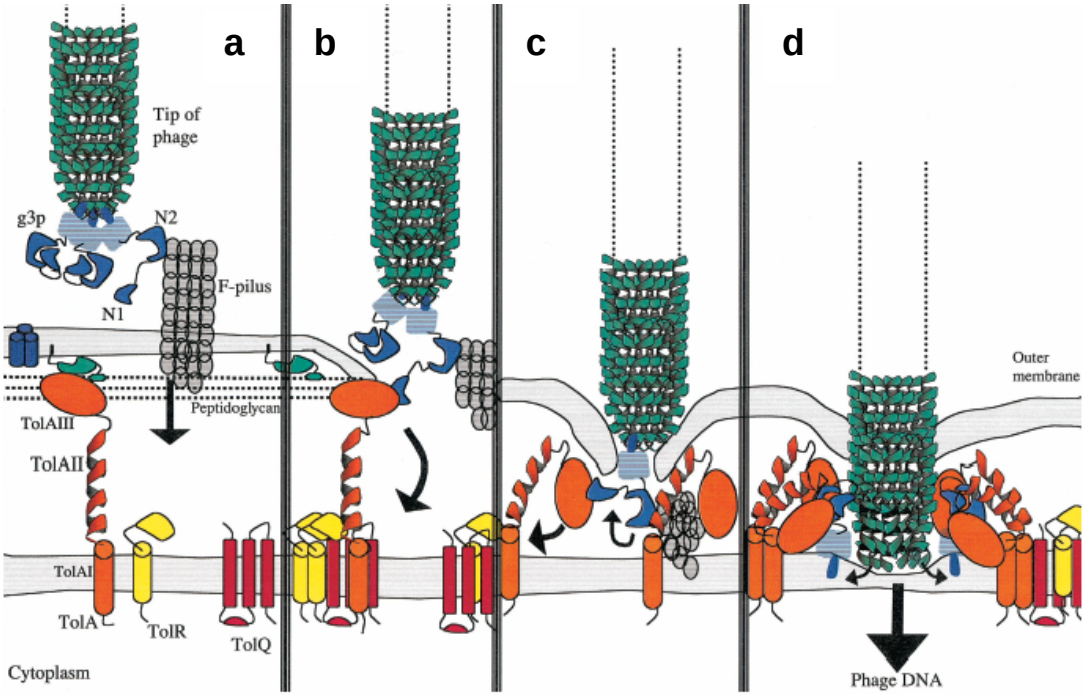


**Figure 1.12:** Model for the early events in the phage infection of E. coli. (Karlsson *et al*., 2003)

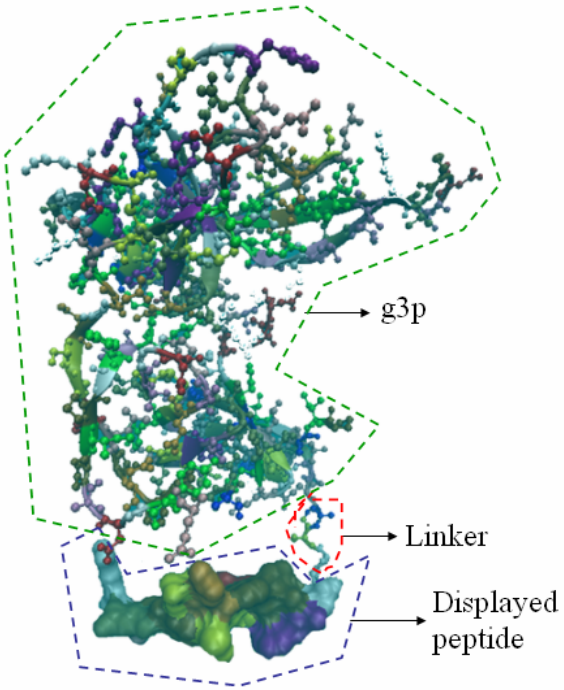


**Figure 1.13:** Computer simulation of the g3p protein of M13 with the displayed peptide on it.

### 1.4. Aim of the Study

In this study our aim has two aspects. The first aspect is to select hydorxyapatite (HA) binding peptides by phage display method using a 7 amino acid constrained Phage-Peptide Library. This includes a detailed analysis of the selected sequences in terms of physico-chemical properties, binding strength and specificity which would lead to obtain the best binders capable of biomimetic applications. The second aspect of our study is to investigate the possible effects of the selected hydroxyapatite binders on *in vitro* Ca-P mineral synthesis under biological conditions.

## 2. MATERIALS AND METHODS

### 2.1. Materials

#### 2.1.1. Bacterial Strain

*E.coli* ER2738, F´ *lacI*$^{q}$ *Δ(lacZ)M15 proA*$^{+}$*B*$^{+}$ *zzf::Tn10(Tet*$^{R}$*)/fhuA2 supE thi Δ(lac-proAB) Δ(hsdMS-mcrB)5 (*$r_k^-$ $m_k^-$ *McrBC*$^{-}$*)* was used as host strain of M13KE bacteriophage. This strain is not a competent strain and it was included as 50 % glycerol culture in the Ph.D.-C7C Phage Display Peptide Library Kit, (2003).

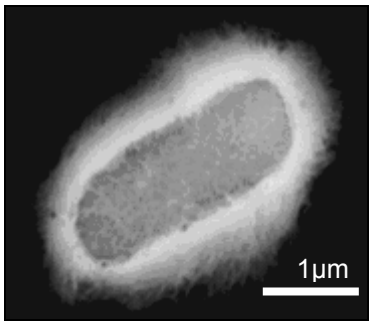


**Figure 2.1:** TEM image of a single *E.coli* ER2738 cell at 24,000X magnification. (Stained with 2% Ammonium Molybdate)

#### 2.1.2. Phage - Peptide Library

Commercailly available Ph.D.-C7C™ Phage Display Peptide Library Kit (New England BioLabs Inc., USA) was used for the selection of HA binding peptides. The library is produced by displaying random constrained heptapeptides on the pIII coat protein of M13KE phage. The library is supplied in 100 µl TBS and 50 % glycerol, with 1.5 x $10^{13}$ pfu/ml. The libraries complexity is ~ 2.7 x $10^{9}$. The library was purchased within Ph.D.-C7C™ Phage Display Peptide Library Kit, Catalog #E8100S.

M13KE is a derivative of M13mp19 designed for expression of peptides as N-terminal pIII fusions in phage display applications (Zwick *et al*. 1998). Relative to the parent M13mp19, Acc65 I/Kpn I and Eag I sites have been introduced flanking the pIII leader peptidase cleavage site, and the Acc65 I/Kpn I site in the multiple cloning site (MCS) was deleted. Random peptide libraries are constructed by annealing an extension primer to a synthetic oligonucleotide encoding the random peptide library

and a portion of the pIII leader sequence, extending with DNA polymerase, and digesting with Acc65 I and Eag I (Noren and Noren, 2001) (Figure 2.2.). The resulting cleaved duplex is inserted into M13KE which has been digested with the same enzymes. M13KE and the insert extension primer are supplied with the Ph.D.-C7C™ Phage Display Peptide Library Kit.

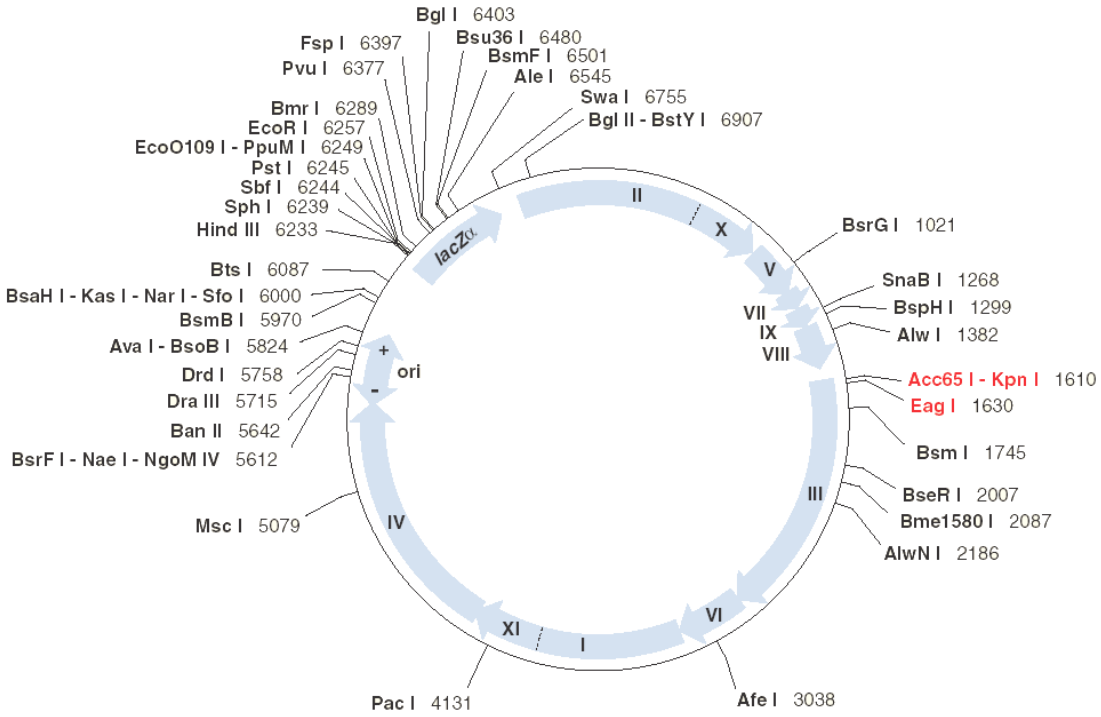


**Figure 2.2:** Restriction map of M13KE (Noren and Noren, 2001).

The randomized segment of the Ph.D.-C7C™ Phage Display Peptide Library is flanked by a pair of cysteine residues, which are oxidized during phage assembly to a disulfide linkage, resulting in the displayed peptides being presented to the target as loops. (Figure 2.2.) The randomized peptide sequences in the library is expressed at the N-terminus of the minor coat protein pIII, resulting in a valency of 5 copies of the displayed peptide per virion. The first randomized position in the Ph.D.-C7C library is preceded by Ala-Cys. The library contains a short linker sequence (Gly-Gly-Gly-Ser) between the displayed peptide and pIII.

### 2.1.3. Target Substrate

Synthetic HA powder with specific density of 3.0556 g/cc, average particle size of 287.520 µm, surface area of 10.57 $m^2$/g and surface charge of –19.9 mV was used as target substarte (Figure 2.3.). The powder was obtained from Ivan Transevica Institute, Department of Materials Science, Ukraine.

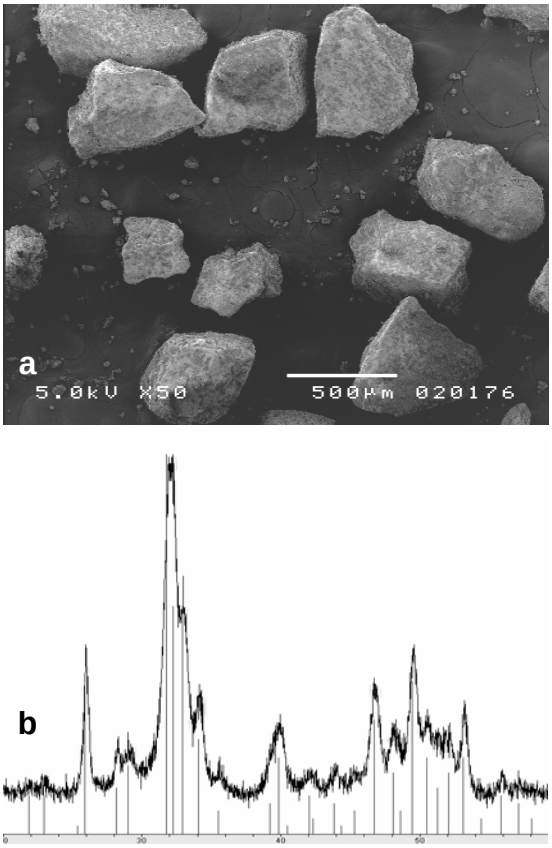


**Figure 2.3: (a)** SEM image of synthetic HA powder used as target substrate. **(b)** XRD pattern of the synthetic HA powder used as target substrate

### 2.1.4. Solutions & Medias

#### 2.1.4.1. Luria Bertani (LB) Medium

10 g tryptone (Acumedia), 5 g yeast extract (Acumedia), 5 g NaCl (Riedel-de-Haen) were dissolved in distilled water and completed up to 1 lt. The pH was adjusted to 7.0-7.5 with 10 M NaOH and sterilized for 15 min. under 1.5 atm at 121 ˚C. The medium was stored at room temperature.

#### 2.1.4.2. LB Agar Medium

10 g tryptone (Acumedia), 5 g yeast extract (Acumedia), 5g NaCl (Riedel-de-Haen), 15 g bactoagar (Acumedia) were dissolved in distilled water and completed up to 1lt The pH was adjusted to 7.0-7.5 with 10 M NaOH and sterilized for 15 minutes under 1.5 atm at 121˚C. Following autoclaving, tetracycline solution (Sigma) (final concentration of 10 µg/ml) and X-gal/IPTG solution (final concentration of 40 µg/ml) (Fermentas/Sigma) were added when the temperature of the medium was cooled down to 45-50 ºC. The medium was shaken properly and poured into the plates by avoiding any bubble formation (3.5 ml for 60mm plates and 15 ml for 100mm

plates). After the medium was solidified in the plates, they were turned upside down and stored at 4 ˚C and protected from light for later use.

#### 2.1.4.3. Top-Agar Medium

10 g tryptone (Acumedia), 5 g yeast extract (Acumedia), 5 g NaCl (Riedel-de-Haen), 1 g $MgCl_2$ (Riedel-de-Haen), 9 g LMP (Low Melting Point) agarose (Acumedia) were dissolved in distilled water and completed up to 1 lt and sterilized for 15 minutes under 1.5 atm at 121 ˚C. The medium was stored at room temperature and melted in microvawe as needed to pour onto the LB agar plates.

#### 2.1.4.4. ER2738 Overnight Culture

5 ml LB solution containing 1 mM $MgCl_2$ and tetracycline, was inoculated with *E. coli* ER-2738 stock (from -80°C). The culture was left in the shaker overnight at 37°C, 200 rpm.

#### 2.1.4.5. Tetracyline-HCl Stock Solution

20 mg/ml tetracycline-HCl (Sigma) was dissolved in distilled water. The solution was stored at -20°C and protected from light.

#### 2.1.4.6. Xgal/ IPTG Stock Solution

1.25 g IPTG (isopropyl β-D-thiogalactoside) (Sigma) and 1 g Xgal (5-Bromo-4-chloro-3 indolyl-β-D-galactoside) (Fermentas) were dissolved in 25 ml Dimethyl formamide (Riedel-de-Haen). The solution was stored at -20°C and protected from light.

#### 2.1.4.7. Detergent Stock Solution

20 % (w/v) Tween 20 (Riedel-de-Haen) and 20 % (w/v) Tween 80 (Merck) were mixed and dissolved in 20 ml distilled water.

#### 2.1.4.8. Glycerol Stock Solution

80 ml of 100% glycerol (Sigma) was mixed with distilled water up to 100 ml total volume to have 80 % glycerol solution. It was sterilized for 15 minutes under 1.5 atm at 121˚C and stored at room temperature.

#### 2.1.4.9. $MgCl_2$ Stock Solution

1M $MgCl_2.6H_2O$ (Fisher) was dissolved in distilled water up to 100 ml. and sterilized with 0.2 µm single use syringe filter.

#### 2.1.4.10. PEG / NaCl Solution

20% (w/v) polyethylene glycol-8000 (PEG-8000) (Sigma), 2.5 M NaCl (Sigma) were prepared in distilled water up to 100ml and sterilized for 15 min under 1.5 atm at 121˚C. The solution was stored at room temperature.

#### 2.1.4.11. PC Buffer (Potassium Phosphate-Sodium Carbonate Buffer)

**PC Buffer (no detergent):** 55 mM $KH_2PO_4$ (Fisher), 45 mM $Na_2CO_3$ (Fisher), 200 mM NaCl (Sigma) were prepared in distilled water and the solution was sterilized by 0.2 µm single use syringe filter. The pH was adjusted to 7.2-7.5.

**PC Buffer (0.02% detergent):** 55 mM $KH_2PO_4$ (Fisher), 45 mM $Na_2CO_3$ (Fisher), 200 mM NaCl (Sigma), 0.5 ml detergent stock solution were prepared in distilled water and the solution was sterilized by 0.2 µm single use syringe filter. The pH was adjusted to 7.2-7.5.

**PC Buffer (0.1% detergent):** 55 mM $KH_2PO_4$ (Fisher), 45 mM $Na_2CO_3$ (Fisher), 200 mM NaCl (Sigma), 2.5 ml detergent stock solution were prepared in distilled water and the solution was sterilized by 0.2 µm single use syringe filter. The pH was adjusted to 7.2-7.5.

**PC Buffer (0.5% detergent):** 55 mM $KH_2PO_4$ (Fisher), 45 mM $Na_2CO_3$ (Fisher), 200 mM NaCl (Sigma), 12.5 ml detergent stock solution were prepared in distilled water and the solution was sterilized by 0.2 µm single use syringe filter. The pH was adjusted to 7.2-7.5.

**Note:** PC buffer can not be sterilized by autoclaving because $CO_3^-$ ions are converted to $CO_2$ due to high pressure during the autoclave. This conversion causes an increase in pH up to 10.

#### 2.1.4.12. Elution Buffers

**Elution buffer I:** 0.2 M glycine (Merck) and 1mg /ml BSA (Sigma) were dissolved in distilled water and pH was adjusted to 2.2 with 10 M HCl and 0,1M HCl. The solution was sterilized by 0.2 µm single use syringe filter.

**Elution buffer A:** 0.2 M glycine (Merck) and 2 mg /ml BSA (Sigma), 0.02% SDS were dissolved in distilled and pH was adjusted to 2.2 with 10 M HCl and 0.1 M HCl. The solution was sterilized by 0.2 µm single use syringe filter.

**Elution buffer B:** 1 M NaCl (Riedel-de-Haen), 100 mM DDT (Sigma), 7 mM TCEP (Sigma), 100 mM ME were dissolved in distilled water.

**Elution buffer II:** Elution buffer A and B were mixed at 1:1 ratio and the solution was sterilized by 0.2 µm single use sterile syringe filter.

#### 2.1.4.13. Tris Buffer

5% Casein (Sigma), 10 mM Tris-base (Merck), 150 mM NaCl, 1% tween 20 (Riedel-de-Haen) were dissolved in 0.1 M NaOH. pH was adjusted to 8.2.

#### 2.1.4.13. TBE (Tris / Borate / EDTA) Solution

10X TBE buffer was prepared by dissolving 108 g tris-base (Merck), 55 g boric acid (Riedel-de-Haen.) and 4 % (v/v) 0.5M EDTA (Merck) in distilled water. pH was set to 8.0.

### 2.1.5. Laboratory Equipments

**Autoclave:** Yamato sterilizer SE 510.

**Electronic balance:** Denver Toledo AB 54

**Centrifuge:** Sorvall RC 5B Plus Kendro Laboratory Products Eppendorf Centrifuge 5415D

**Centrifuge rotors:** SA-600, SLA-1500, SH-3000, PN-11779.

**Deep freezes and refrigerators:** Heto Polar Bear 4410 ultra freezer, JOUAN Nordic A/S, catalog# 003431.

**Deionized water system:** Millipore Milli Q Synthesis A 10

**Fluorescence microscope:** Nikon Eclipse TE 2000-U

**Glassware:** Technische Glaswerke Ilmenau GmbH.

**Ice machine:** Cornelius Ice Systems

**Incubators:** Quincy Lab. Inc. Model 10-14 Incubator VWR 1310

**Laminar flow cabinet:** Airclean 600 PCR Workstation ISC Bioexpress

**Orbital shaker:** Innova 3100 Water Bath Shaker New Brunswick Scientific

**Magnetic stirrer:** AGE 10.0164, VELP Scientifica srl.**:** ARE 10.0162, VELP Scientifica srl.

**Automatic pipettes:** Pipetteman 1-20-200-1000-5000 ml

**pH meter:** MP 220, Mettler Toledo International Inc.**:** Inolab pH level 1, order# 1A10-1113,Wissenschaftlich-Technische Werkstätten GmbH & Co KG.

**PCR cycler:** Eppendorf Master Cycler Gradient

**Power supply:** EC 250-90, E-C Apparatus

**DNA sequencer:** Applied Biosystems 3730XL

**Spectrophotometer:** Tecan Safire

**TEM:** Philips 420 EM

**Transilluminator:** UV Transilluminator 2000, Catalog# 170-8110EDU, Bio-Rad.

**Ultrasonic bath:** Branson 1200

**Vacuum Dryer:** Eppendorf Vacufuge Vacuum Pump: Vacuum Station, Catalog# 165-5004, Bio- Rad.

**Vortexing machine:** Reax Top, product# 541-10000, Heidolph2.2.

**X-ray diffractometer:** PW1820 Diffractometer coupled with PW1830 Generator, Philips

## 2.2. METHODS

### 2.2.1. Biopanning

Shortly, one panning round consists of 5 main steps: i-incubating the phage peptide library with the target substrate, ii-removing the non-specifically or weakly bound and unbound phage particles, iii-eluting the specifically-bound phages, iv-amplifying the eluted phage, v-selection of single clones and sequencing. The eluted and amplified phages can be used for additional panninng rounds to enrich the pool in favor of binding sequences. In this study 3 rounds of panning were performed. A brief procedure of panning of the phage peptide library against synthetic HA powder is given in Figure 2.4.

#### 2.2.1.1. Cleaning the HA Powder

Carefully weighed 10 mg powder was suspended in 100 μl distilled water and 900 μl of 1:1 $CH_3OH$ / $CH_3COCH_3$ mixture was added to the suspension. After vortexing 5 minutes, the suspension was sonicated for 20 minutes in an ultrasonic bath to break the powder clusters. Then the suspension was centrifuged at 200 G for 3 minutes and the supernatant was removed. The powder was re-suspended in 1 ml $(CH_3)_2CHOH$ and sonicated for 20 minutes. After vortexing 5 minutes, the suspension was centrifuged at 200 G for 3 minutes. The supernatant removed and the powder was resuspended in 1 ml PC buffer containing 0.5 % detergent. After

vortexing 5 minutes, the suspension was sonicated for 60 minutes. After the sonication the suspension was quickly vortexed and centrifuged at 200 G for 3 minutes. The supernatant was removed and the powder was re-suspended in PC buffer containing 0.5 % detergent. Then the powder was washed twice with distilled water and twice with $(CH_3)_2CHOH$. The powder was dried at vacuum.

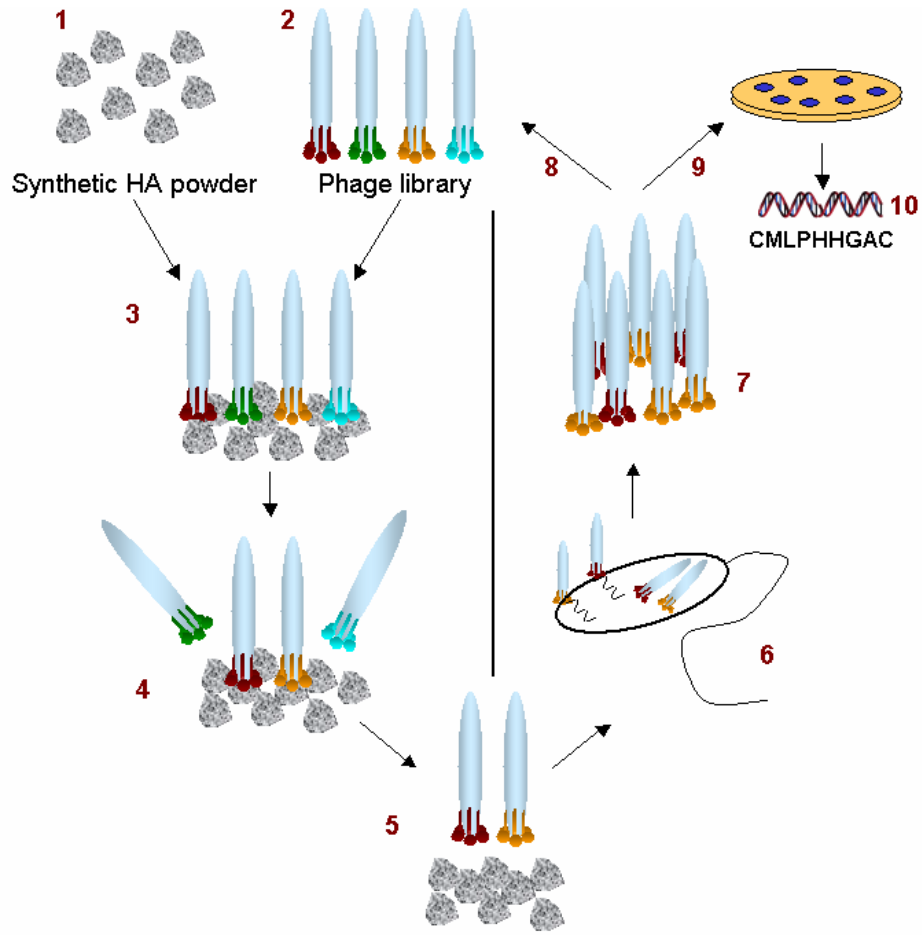


**Figure 2.4:** Phage display procedure (The sizes are not to scale): **1)** Cleaned polycrystalline HA powder. **2)** Ph.D.-C7C™ Phage Display Peptide Library. (Different colors representing different random sequences. **3)** The library is incubated with the HA powder in potassium PC bufer containing 0.1% detergent. **4)** Unbound phages are removed by washing with PC buffer containing 0.1% detergent. **5)** Specifically bound phages are eluted from the surface using elution buffers **6)** The eluted phage pool is amplified with *Eschericia coli* ER2738. **7)** Amplified phages are purified. Amplified and purified phages are used for **8)** additional panning rounds and **9)** after each round the phages are grown on solid media and single clones are selected by picking single phage plaques. **10)** DNA of single phage clones are isolated and sequenced. Since the insert position of the random sequences are known, the peptide sequenced displayed on each clone can be obtained from the DNA sequences.

### 2.2.1.2. Phage – Peptide Library Incubation With HA Powder

1 mg of cleaned HA powder was suspended in 990 μl PC buffer containing 0.1 % detergent and 10 μl of phage peptide library was added to the suspension. The suspension was left overnight at room temperature with constant rotating. The detergent in the buffer prevents the non-specific interactions between phages and provides the phages to interact with the powder surface individually.

### 2.2.1.3. Washing Un-bound Phages

After overnight incubation with phage peptide library, the suspension was centrifuged at 200 G for 3 minutes. The supernatant, containing unbound or non-specifically bound phages, was transferred to a fresh tube and the powder was re-suspended in 1 ml PC buffer containing 0.1 % detergent. The suspension was rotated for 30 minutes. At this step, non-specifically bound phages are removed from the surface. After 30 minutes rotation, the suspension was centrifuged at 200 G for 3 minutes. The re-suspending, rotating and centrifuging steps were repeated 11 times (Figure 2.5.). The supernatant, containing unbound or non-specifically bound phages, was collected to a fresh tube at each repeat.

The washing procedure was the same for each round of panning except for the 4$^{th}$ round. At the 3$^{rd}$ round PC buffer containing 0.5% detergent was used instead of 0.1%, to obtain the strongest binders by making the washing environment harsher.

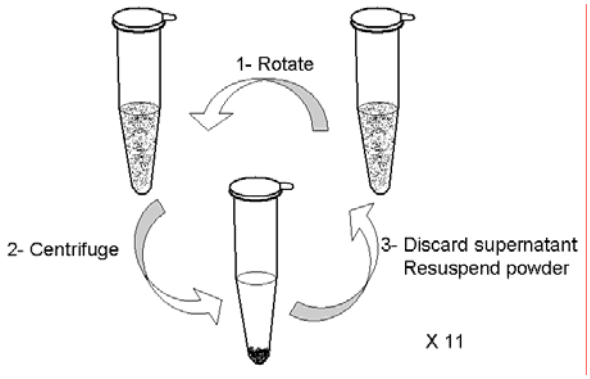


**Figure 2.5:** Procedure of washing

### 2.2.1.4. Recovery of the Bound Phages

After washing the powder to remove the un-bound phages, strongly bound pahges were recovered from the powder surface. A newly developed physical elution method was used beside chemical elution to improve the efficiency of recovery. In

the chemical elution, phages are removed from the surface by creating a harsh environment by low pH elution buffers. In the physical elution, phages are recovered by sending ultrasonic waves to the powder suspension and removing the phages from the surface physically. The phages must not be kept in the elution buffer longer than 15 minutes since the pH of elution buffers are 2.2 and phage particles lose their viablity at this low pH. At the end of all elution steps, the powder was resuspended in PC buffer and transferred to a fresh *E. coli* ER2738 mid log culture in order to amplify the phages remained on the surface after all elution steps

#### 2.2.1.5. Chemical Elution

After the last washing step, the powder was re-suspended in 1 ml of Elution Buffer I and rotated for 15 minutes. After 15 minutes rotation the suspension was centrifuged at 200 G for 3 minutes. 800 µl of the supernatant was transferred to 50 ml fresh *E. coli* ER2738 mid log culture. The incubation of the culture was started right after adding the supernatant. The remaining 200 µl of the supernatant was neutralized by adding 40 µl Trish Buffer (pH:9.1). Powder was re-suspended in 1 ml of Elution Buffer II and rotated for 15 minutes. After 15 minutes rotation the suspension was centrifuged at 200 G for 3 minutes. 800 µl of the supernatant was transferred to 50 ml fresh *E. coli* ER2738 mid log culture. The incubation of the culture was started right after adding the supernatant. The remaining 200 µl of the supernatant was neutralized by adding 40 µl Trish Buffer (pH:9.1). The powder was re-suspended in Elution Buffer II and the same procedure was repeated 2 more times, resulting in 4 steps of elution. In each step, the supernatant was transferred to a fresh *E. coli* ER2738 mid log culture.

#### 2.2.1.6. Physical Elution

After the $4^{th}$ step of chemical elution, the powder was re-suspended in 1 ml PC buffer. The tube was placed in an ice bath and ultrasonicated using an ultrasonic probe at 150 W and 20 kHz (Braunsonic, U. Waves Probe, USA). At the $15^{th}$ second of the sonication, 800 ml of the suspension was collected and centrifuged at 200 G for 3 minutes. The supernatant was transferred to a fresh *E. coli* ER2738 mid log culture. The powder was re-suspended in LB media and transferred to a fresh *E. coli* ER2738 mid log culture to amplify the phages remained on the powder after all elution steps.

### 2.2.1.7. Amplification of the Recovered Phages

*E. coli* ER2738 mid log cultures, which eluted phages were added to, were incubated at 37$^{o}$C for 4 hours with constant orbital shaking at 200 rpm. During this time, M13 phage particles infect *E. coli* cells and new phage particles are produced. Phage particles bind to *E. coli* through the F pilus. After binding to the phage, the pilus retracts, bringing the phage particle to the cell surface. There, the N-terminal domain (N1) of pIII interacts with the membrane-bound protein, TolA. The single-stranded DNA (plus strand) of the phage particle enters the bacterial cell through a process that is not well-understood, and it is then converted to double-stranded DNA (replicative form) by *E. coli* proteins. Two virally encoded proteins, pII and pX, are involved in rolling-circle amplification of the double-stranded viral genome, which leads to the production of plus-strand copies of the phage DNA. Such progeny molecules are then coated by the single-strand DNA binding protein, pV. The DNA-protein complex interacts with the export machinery (pI, pIV, pXI, and thioredoxin), which simultaneously assembles and secretes viral particles using a pool of phage coat proteins that have already been inserted into the inner membrane. Finally, the viral particle is released from the cells, without killing them, and pV is recycled. (Figure 2.6.) The cultures may not be incubated longer than 4.5 hours since longer incubation periods will cause mutations in the phage genome causing the change or loss of the displayed peptide.

### 2.2.1.8. Purification of Amplified Phages

At the end of 4 hours of growth period, *E. coli* - phage cultures were transferred into 250 ml sterilized polypropylene centrifuge tubes. The cultures were centrifuged at 8,000 rpm for 10 min. At this step the cells are spinned down and the phage particles remain in the supernatant. The supernatants were transferred to a fresh 250 ml sterilized polypropylene centrifuge tube. 8.33 ml of PEG / NaCl solution was added to the supernatant and was left overnight at 4 $^{0}$C. At this step the phage particles are precipitated out from the solution. After overnight waiting, the tubes were centrifuged 8,000 rpm for 10 minutes. Supernatants were discarded and phage pellets were resuspended in 5 ml PC buffer. The tubes were centrifuged at 8,000 rpm for 10 minutes. At this step any remaining *E.coli* cells are spinned down. Supernatants were transferred into 50 ml sterilized polypropylene centrifuge tubes. 0.833 ml of PEG / NaCl was added to the solution to precipitate phage and the solution was kept at 4 $^{0}$C for 2 hours. Tubes were centrifuged at 10,000 rpm for 10 minutes. Supernatants were discarded and phage pellets were resuspended by in 1 ml PC buffer. Tubes were centrifuged at 10,000 rpm for 10 minutes and

supernatants were transferred into sterilized microfuge tubes. 0.166 ml of PEG / NaCl solution was added to the microfuge tubes to precipitate phage and the tubes were vortexed for 5 sec, and kept at room temperature for 10 minutes. Tubes were centrifuged at 13,500 rpm for 1.5 minutes to get the compact phage. Supernatants were discarded and phage pellets were re-suspended with 0.2 ml PC buffer by pipetting gently. The tubes were centrifuged at 13,500 rpm for 1.5 minutes. Supernatants, containing ~$10^{11}$ pfu M13, were transferred into fresh sterilized microfuge tubes, labeled properly and stored at $4^0$C.

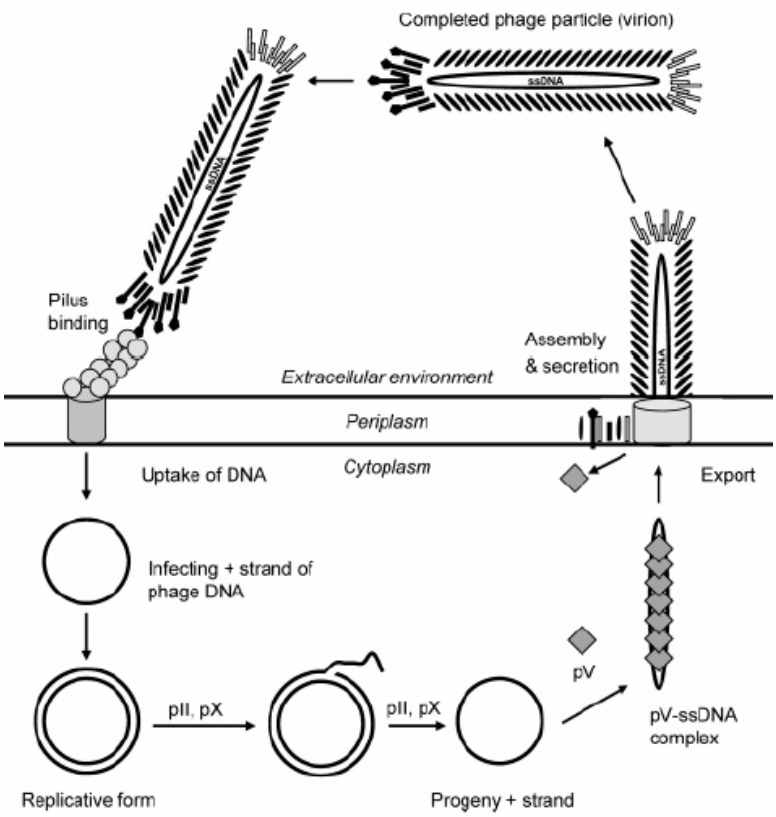


**Figure 2.6:** Life cycle of M13 (Kehoe and Kay, 2005)

### 2.2.2. Selection of Single Colonies - Blue- White Screening

After purifying the phages from each round, single colonies were selected by blue-white display. ER2738 strain of *E.coli* lacks the lac Z $\alpha$ gene. By the infection of the M13mp 19 phage, carrying the lacZ $\alpha$ gene, the ER2738 cells can produce competent $\beta$-galactosidase. X-gal is a chromogenic substrate for $\beta$-galactosidase. A blue color forms when X-gal is hydrolized by $\beta$-galactosidase so blue phage plaques form on X-gal / IPTG containing plates by the metabolism of X-gal.

### 2.2.2.1. Preparation of mid-log *E. coli* Cultures

2 ml media was prepared by adding 4 μl of 1M $MgCl_2$ and 2 μl of tetracycline stock solution to LB media. 5 μl of fresh *E. coli* overnight culture was added to the media and the culture was incubated at 37°C untill the OD reached to 0.5.

### 2.2.2.2. Plating Cell-Phage to Solid Media

Several dilutions of the phages were prepared prior to screening in order to obtain single plaques. The dilutions were prepared in a standart 96 well ELISA plate. 90 μl PC buffer was put into the first well of the plate. 180 μl PC buffer was put into the other wells. 10 μl phage stock solution was added into the first well resulting $10^{-1}$ dilution. Phage and PC buffer were mixed by pipetting. 20 μl sample was taken from the first well and put into the second well to have totally 200 μl of solution resulting $10^{-2}$ dilution level of the phages. The remaining serial dilutions were done the same way. (Figure 2.7.)

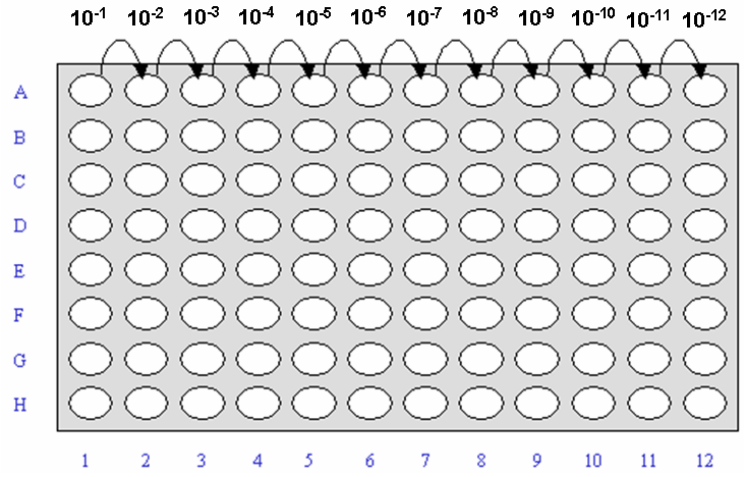


**Figure 2.7:** Making the serial dilutions on the Elisa plate

Overnight culture of ER2738 was prepared one night before plating the phages. Previously prepared LB Agar plates containing X-Gal / IPTG were brought to room temperature. Top agar media was melted in a 50°C water bath. 20 μl of diluted phage solution was added to 180 μl LB solution containing *E. coli* cells with $OD_{600}$ ~ 0.5 resulting in another 10 times dilution of the phage solution making the final dilution $10^{-3}$. The phage-cell mixture was added to warm LB agar (0.5 μl for 60 mm Petri dishes and 3.5 μl for 90 mm Petri dishes) in 15 ml falcon tubes and vortexed. The mixture was poured onto the LB plates and waited for 5-10 min for the

solidification of the top agar. After the top agar froze, all Petri dishes were turned upside down and incubated at 37°C for 8-14 hours. Turning the plates upside down provides formation of single phage plaques.

#### 2.2.2.3. Phage Titers for Each Round

At the end of the each round, phage titers was estimated by blue-white screening. After single phage plaques were obtained, the colonies were counted on the plates and the titers of the phages were approximately calculated multiplying with the dilution factor.

#### 2.2.2.4. Preparation of Glycerol Stock of Phage

After single phage plaques were obtained, plagues were picked and kept in glycerol for sequencing and further analysis. The plaques were picked by a sterile pipette tip and placed into 200 μl PC buffer containing 0.02 % detergent. Then the buffer was kept at 60°C for 45 minutes to dissolve any residual LB Agar on the plaque. Then glycerol stocks were prepared for long storing of the phage clones. 60 μl sterilized 80% glycerol solution was put into each well of a fresh 96-well plate. Then 50 μl of single phage plaque dissolved in PC buffer was added into glycerol, resulting a ~50% glycerol stock. The stocks were kept at -80°C

### 2.2.3. Characterization of the Phage Clones – DNA Sequencing

For the sequencing of the individual phage cones, DNA of each clone was isolated. Commercially available QIAprep ® Spin M13 kit (QIAGEN, Catolog #27704) was used for the isolation of M13 ssDNA. First, the phages were amplified for DNA isolation. 50 μl from each individual phage plaque was taken from the glycerol stock and added into 2 ml *E. coli* ER2738 mid-log culture in a 2ml microfuge tube. Phages were amplified for 4 hours at 37°C. At the end of the 4 hours, microfuge tubes were centrifuged at 5000 rpm for 15 min at room temperature. Supernatant containing M13 bacteriophage was transferred into a fresh reaction tube without disturbing the pellet which contains the cells. Any carryover of bacterial cells will result in contamination of the M13 ssDNA with bacterial chromosomal DNA or double-stranded bacteriophage RF DNA. Buffer MP was added at a 1/100 ratio to the supernatant in the reaction tube and was mixed by vortexing. The mixture was incubated at room temperature for at least 2 minutes. During this step, bacteriophage particles were precipitated from the culture medium. A QIAprep spin column was placed in a fresh 2 ml microcentrifuge tube and 0.7 ml of the precipitated phage was transferred to the QIAprep spin column. Reaction tube was

centrifuged for 15 s. at 8,000 rpm and the flow through collected at the bottom was discarded. At this step, intact bacteriophage was retained on the silica-gel membrane of the spin column. This step was repeated until all of the precipitated phage was passed through QIAprep spin column. 0.7 ml MLB buffer was added on the spin column for M13 lysis and was and centrifuged for 15 seconds at 8,000 rpm. This step creates appropriate conditions for binding of the M13 ssDNA to the QIAprep silica-gel membrane. Another 0.7 ml MLB buffer was added to the spin column and incubated for 1 minute at room temperature to lyse the bacteriophage completely. Spin column was centrifuged for 15 seconds at 8,000 rpm. 0.7 ml Buffer PE was added to the spin column and the column was centrifuged for 15 seconds at 8,000 rpm to remove any residual salt. Buffer PE was discarded from collection tube and the spin column was centrifuged for 15 seconds at 8,000 rpm to remove residual buffer PE. It is important not to dry the spin column membrane with quick microcentrifugation steps since any residual ethanol carried over will affect the subsequent PCR steps.

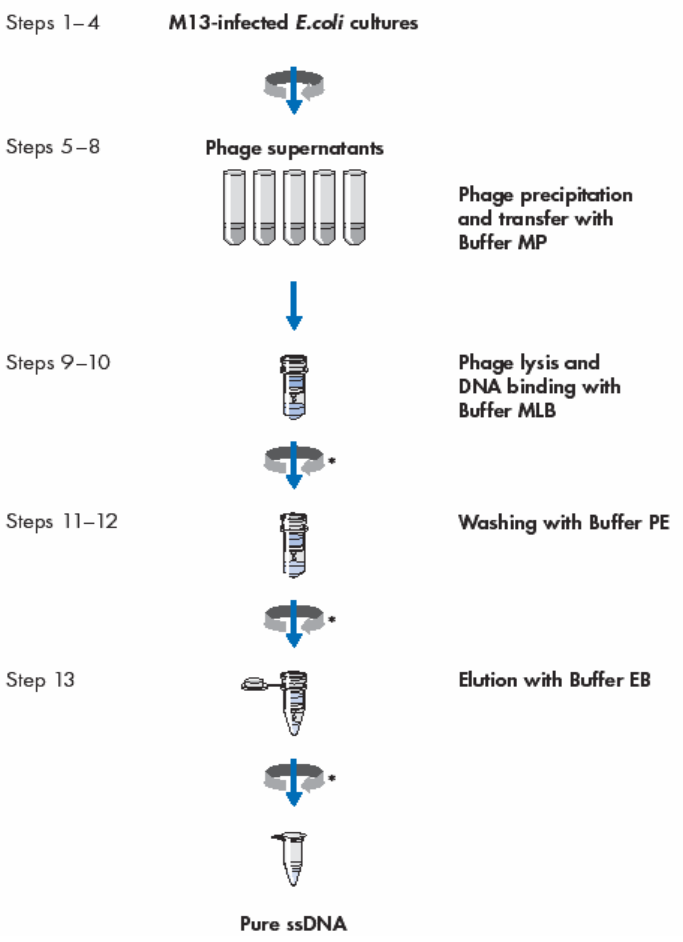


**Figure 2.8 :** M13 ssDNA isolation procedure (QIAGEN, Catolog #27704).

The spin column was placed in a fresh 1.7 ml microcentrifuge tube. 100 µl Buffer EB (10 mM tris.Cl, pH 8.5) was added to the center of the column membrane to elute the ssDNA from the membrane. After 10 min of incubation at room temperature, the tube was centrifuged for 30 seconds at 8,000 rpm to collect the isolated ssDNA.

#### 2.2.3.1. PCR Conditions for DNA Sequencing

PCRs were done at a total volume of 10 µl in 0.2 ml PCR reaction tubes. Big dye ® terminator v3.1 cycle sequencing Kit (Applied Biosystems) was used for the sequencing PCRs.

**Table 2.1:** PCR conditions used for DNA sequencing

| PCR ingredients | Amount |
|---|---|
| Big dye reaction mix* | 1µl |
| 5X sequencing buffer / dd$H_2O$ | 3 µl |
| Template ssDNA | 2 µl (150 ng) |
| Primer (-96 sequencing primer) * | 3.2 µl (3.2 pmol) |
| d$H_2O$ | 0.8 µl |
| **Total volume** | **10 µl** |

* –96 gIII sequencing primer (5´- HOCCC TCA TAG TTA GCG TAA CG –3´, 100 pmol, 1 pmol/µl) was supplied with the New England Biolabs Ph.D.-C7C™ Phage Display Peptide Library Kit

PCR conditions for cycle sequencing were as follows; 95 ºC – 2 minutes, 95 ºC – 10 minutes, 55$^{O}$C – 10 minutes 60$^{O}$C – 4minutes. The reaction was run for 35 cycles.

#### 2.2.3.2. Purification of PCR Product

2 µl of 3M sodium acetate (pH 4.6) and 50 µl 95 % ethanol were mixed for each sample. 52 µl of this mixture was added into each PCR product and samples were incubated on ice for 30 minutes. After incubation, samples were centrifuged for 30 minutes at 14000 rpm. Supernatant was discarded and DNA pellet was washed with 250 µl cold ethanol. Samples were centrifuged for 30 minutes at 14000 rpm. Residua ethanol was discarded by evaporating at 95$^{o}$C. DNA was re-dissolved in 20 µl di-formamide. Samples were denatured by keeping at 95$^{o}$C and then at -20$^{o}$C for 5 minutes. ABI 3100 Avant (PE, Applied Biosystem, CA) automated sequencer was used for DNA sequencing.

### 2.2.4. Characterization of the Phage Clones – Immunofluorescence Microscopy

After obtaining the amino acid sequences displayed on phage clones by DNA sequencing, immunofluorescence microscopy was done to determine the binding strength of the each clone. The same powder substrate used for the phage display selection was used for immunofluorescence microscopy. First the phage clone and the powder was incubated. Then the phages on the powder were labeled with Anti-M13 IgG and Anti M13 IgG was labeled with FITC-Anti IgG Fab conjugate. Then the powder was checked under the microscope. (Figure 2.9.)

#### 2.2.4.1. Labeling

1 mg of previously cleaned HA powder was suspended in 990 μl PC buffer containing 0.1 % detergent. Then 10 μl phage was added to the suspension from a $10^{13}$ PFU/ml in PC buffer containing 0.1 % making a final phage concentration of $10^{11}$ PFU/ml. The phage and powder suspension was incubated overnight at room temperature with constant rotating. After the overnight incubation, primary antibody (Anti M13 IgG) and secondary antibody (Anti IgG Fab – Alexa-Fluor conjugate) complex was prepared by mixing at 1:5 ratio and incubating 30 minutes. Anti M13 IgG binds specifically to the g8p (major coat protein) of the phage and the Alexa-Fluor – Anti IgG conjugate binds to the Anti M13 IgG. Therefore, the phage particles become observable under fluorescence light. While the dye mixture is being prepared, overnight incubated phage-powder suspension was centrifuged at 1,000 rpm for 1.5 minutes. The supernatant was discarded and the powder was resuspended in PC buffer containing 0.1 % detergent. The suspension was rotated for 15 minutes and centrifuged again at 1,000 rpm for 1.5 minutes and the supernatant was discarded. The powder was resuspended in 497 μl PC buffer containing 0.1 % detergent and 3 μl of the dye mix was added to the suspension. The tube was covered with aluminum folio to protect the fluorescent dye from the light and was incubated for 30 minutes. At the end of the 30 minutes the suspension was centrifuged at 1,000 rpm for 1.5 minutes and the supernatant was discarded. The suspension was washed three times with PC buffer containing 0.1 % detergent. At the last washing, the supernatant was discarded and the powder was re-suspended in 20 ml of PC buffer containing 0.1 % detergent. Then the suspension was transferred on a clean microscope slide and checked under a Nikon Eclipse TE 2000-U microscope.

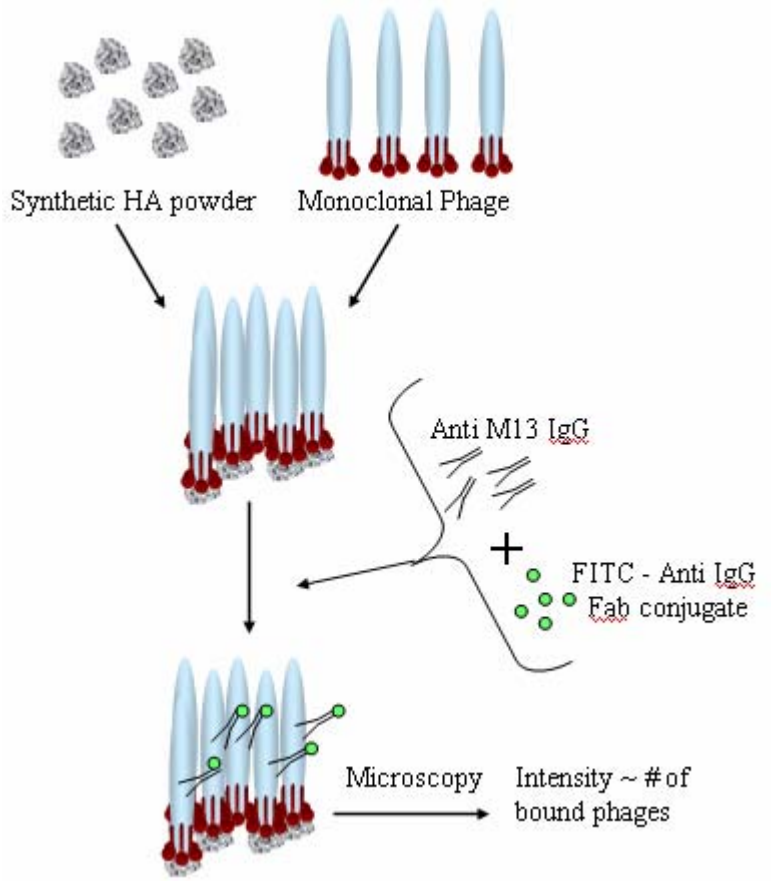


**Figure 2.9:** Labeling procedure for fluorescence microscopy

#### 2.2.4.2. Calculation of the Surface Coverage

The approximate percent binding affinity of the phages were calculated using MetaMorph ® Imaging System Ver. 6.3. First approximate surface area of the powder in bright field image was calculated using the software. Then the area of the emitted fluorescence light was calculated with the same way. Then the percentages were compared and the percent surface coverage of the phages was calculated. The phages were grouped as strong, moderate and weak binders according to their surface coverage.

### 2.2.5. Characterization of the phage clones – ELISA

1 mg of previously cleaned HA powder was suspended in 990 μl PBS buffer containing 2% BSA. Then 10 μl phage was added to the suspension from a $10^{13}$ PFU/ml in making a final phage concentration of $10^{11}$ PFU/ml. The phage and powder suspension was incubated for 2 hours at room temperature with constant rotating. After the incubation, phage-powder suspension was washed 3 times with 200μl PBS buffer containing 0.05% detergent. After the washing, the powder was re-suspended in 200μl PBS buffer containing 2% BSA. Then 0.4μl HRP-AntiM13

antibody conjugate was added to the suspension (Amersham Biosciences, USA) and incubated for 30 minutes at room temperature with constant rotating. After the incubation, the powder was washed for four times with 200µl PBS buffer containing 0.05% detergent After the washing, the powder was re-suspended in 200µl PBS buffer containing 0.05% detergent. Enzymatic reaction was started by adding 100µl TMP (1-step TMP-ELISA, Catalog# 34022, Pierce) to the powder suspension. Reaction was ended after 2 minutes by adding 100µl 1M $H_2SO_4$. The color change was measured with automated multiplate reader (Tecan Trading AG, Switzerland) at 450 nm wavelength. (Figure 2.10)

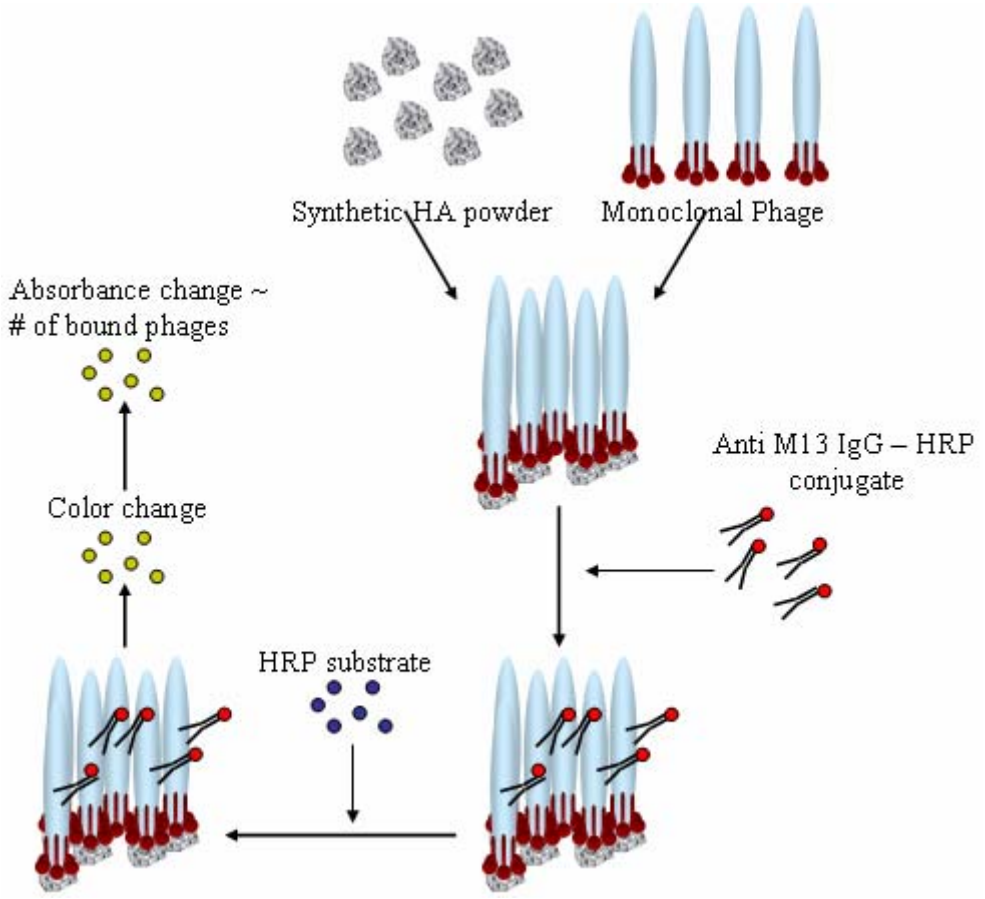


**Figure 2.10:** ELISA protocol

### 2.2.6. *in vitro* Mineralization in the Presence of Binder Phages

An alkaline phosphatase (AP) mediated mineralization system was used for *in vitro* mineralization experiments. In this system $Ca^{+2}$ needed for the mineralization is provided exogenously by dissolving $CaCl_2$. The $PO_4^{-3}$ is provided by e hydrolysis of an organic phosphate compound by AP. Here, β-Glyserophosphate was used as the organic phosphate compound. When $PO_4^{-3}$ is released to the solution, $Ca^{+2}$ and $PO_4^{-3}$ ions form the Ca/P structure (Figure 2.11.)

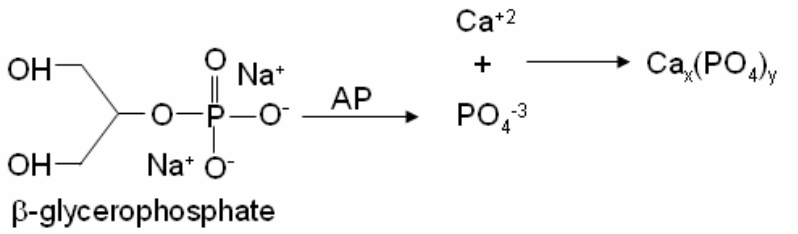


**Figure 2.11:** AP mediated mineralization reaction

#### 2.2.6.1. Mineralization Media

Mineralization media was prepared by dissolving 24 mM $CaCl_2$ and 14.4 mM β-Glycerophosphate (β-GP) in 25 mM Tris-HCl buffer (pH:7.4). 2X media was prepared, filter sterilized and kept at 4°C. The media containing hydroxyapatite binding phages were simply prepared by adding proper amount of phage stock solution to the media stock and completing the final concentration to 1X.

#### 2.2.6.2. Mineralization Reaction

The reactions were run in a standard 96 well plate. Mineralization solutions containing no phage, MG-49 clone MG-63 clone and wt M13 clone were prepared at 200 ml volume as triplicates. The mineralization reactions were started by adding 3.5 μg/ml commercial bacterial AP to the solutions. The mineralization reaction was continuously monitored 37°C by measuring the absorbance change of the solutions due to the mineral formation using an automated multiplate reader (Tecan Trading AG, Switzerland). Samples were collected at different time points for SEM and TEM analysis.

#### 2.2.6.3. SEM and TEM analysis

### 2.2.7. *in vitro* Mineralization in the Presence of Binder Peptides

The same mineralization media and reaction used in the mineralization experiments with phage was used for peptide experiments. The media containing hydroxyapatite binding peptides were simply prepared by adding proper amount of peptide stock solution to the media stock and completing the final concentration to 1X. The phage stocks used in mineralization experiments were prepared in di-$H_20$ to eliminate the effect of the free phosphate in PC buffer.

#### 2.2.7.2. Mineralization Reaction

Prior to the mineralization experiments, AP activity was measured in the presence of no peptide and the binder peptides to check if the AP activity is affected by the presence of the peptides. The reactions were run in a standard 96 well plate. Mineralization solutions containing no peptide, MG-49 at 0.07 mM and 0.4 mM concentrations and MG-63 at 0.07 and 0.4 mM concentrations were prepared at 200 ml volume as triplicates. The mineralization reactions were started by adding 3.5 μg/ml commercial bacterial AP to the solutions. The mineralization reaction was continuously monitored 37$^{o}$C by measuring the absorbance change of the solutions due to the mineral formation using an automated multiplate reader (Tecan Trading AG, Switzerland).

#### 2.2.7.3. Ca and P Measurements

10 μl of the media was collected from the same reactions at 0.25, 0.5, 1, 1.5, 2, 3, 4, 5, 6, 24, 48, 64 and 96 hours. AP was immediately inactivated after sample collection by heating up to 90$^{o}$C for 10 minutes and then cooling down to –20$^{o}$C, to prevent mineral formation after sample collection. The mineralized phase was separated by centrifuging at 9500 G for 10 minutes. Supernatant, containing the unused Ca and β-GP, was transferred to a fresh tube and the mineral pellet was washed three times with di-water to remove excess salts. Then the mineral pellet was dissolved by adding 10% nitric acid. The tubes were kept under constant shaking for 5 minutes to ensure that all of the powder was dissolved.

For the calcium measurements, a standard curve was prepared with known concentrations of $Ca^{+2}$. The samples were neutralized by 0.1M Tris buffer (pH: 9.1). Then 5 ml of dissolved powder was taken and added to the reaction mix of the Ca assay kit (QuantiChrome $^{TM}$ Calcium Assay Kit – Bioassays, USA). The absorbance

change was measured using an automated multiplate reader (Tecan Trading AG, Switzerland).

For the phosphate measurements, a standard curve was prepared with known concentrations of $PO_4^{-3}$. The samples were neutralized by 0.1M Tris buffer (pH: 9.1). Then the phosphate concentration was measured using phosphate assay kit. (PiPer™ Phosphate Assay Kit - Invitrogen Corporation, USA).

#### 2.2.7.4 SEM and TEM Analysis

Mineralized phase for the case of no peptide, MG-63, and MG-49 were collected at 0.5, 1.5, 2.5, 28 and 96 hours for TEM and SEM analysis. 10 μl sample was collected and placed onto a carbon coated TEM grid. The TEM grid was air dried for 1 minute at room temperature. After 1 minute, liquid on the TEM grid was carefully blotted away using a filter paper. Then the TEM grid was vacuum-dried at 60°C for 2 hours and stored in a desiccated container. TEM and SEM analysis were performed on the same samples collected on the TEM grid.

SEM was performed at 10kV using a JSM 7000 (JEOL, Japan) in secondary electron imaging mode, and TEM imaging and diffraction were performed at 120kV using an EMS 420T (Philips, Netherlands).

#### 2.2.7.5. Kinetic Analysis of the Mineralization Reaction

The kinetics of the mineralization reactions in the presence of no peptide and hydroxyapatite binding peptides were calculated using the Ca and P measurements. First 6 hours data of the reactions were used for the calculations. The calculations were made assuming a $1^{st}$ order reaction.

Amorphous to crystalline transformation rate was calculated by simply dividing the $Ca^{+2}$ concentrations to the $PO_4^{-3}$ concentrations for a given time point. The Ca/P ratio was plotted for the first 6 hours.

## 3. RESULTS AND DISCUSSION

Synthetic hydroxyapatite powder (HA) was used as substrate for the selection of HA-specific 7-aminoacid polypeptides from constrained PhD-7 phage display library. Following the biopanning studies, we have analyzed all sequences in terms of their amino acid content to search for any trend along the sequences or any convergence to a specific sequence and deduced their and their physicochemical properties. In the experimental binding characterization, immunolabelling fluorescence microscopy technique was applied to test the binding strength and the specificity of each sequence.

The selected peptides were categorized according to their binding strength mainly in three groups as good, moderate or weak binders. Next, one of strong and the weak HA binders were selected for investigating their effect in vitro biomineralization studies. We have utilized an enzyme mediated reaction to follow the peptide effect on mineral formation via kinetic and morphological analysis.

### 3.1. Biopanning – Phage Display Selection

We have performed 3 biopanning rounds, total of 290 single phage clones were isolated. 56 of these clones were randomly selected for characterization (18 clones from the $1^{st}$ round, 19 clones from $2^{nd}$ and $3^{rd}$ rounds).

### 3.2. Characterization of the Phage Clones

#### 3.2.1. Determination of Binding Affinity to Hydroxyapatite Powder

We have used immunofluoresence microscopy and ELISA assay to characterize the randomly selected 56 sequences in terms of their affinity from three rounds of biopanning. Out of 56 sequenced clones, 12 clones were characterized as strong binder, with a surface coverage higher than 40%, 28 clones were characterized as moderate binder, with a surface coverage between 35% and 10%, and 16 clones were characterized as weak binder with a surface coverage lower than 10% by immunofluorescent microscopy. Examples of immunofluorescent microscopy and ELISA results are shown in Figure 3.1. and Figure 3.2. No binding was observed

when wild type M13 bacteriophage was incubated with hydroxyapatite powder, indicating that there was no background binding of phage coat proteins.

Amino acid sequences, binding affinities and the physicochemical properties of the characterized clones are listed on Table 3.1., Table 3.2. and Table 3.3.

Binding affinity characterizations showed that 8 of the 12 strong binders were selected in the 3rd round of panning, likewise 11 of 16 weak binders were selected in the 1st round of panning, indicating that strong binding clones were enriched in additional panning rounds (Figure 3.3.).

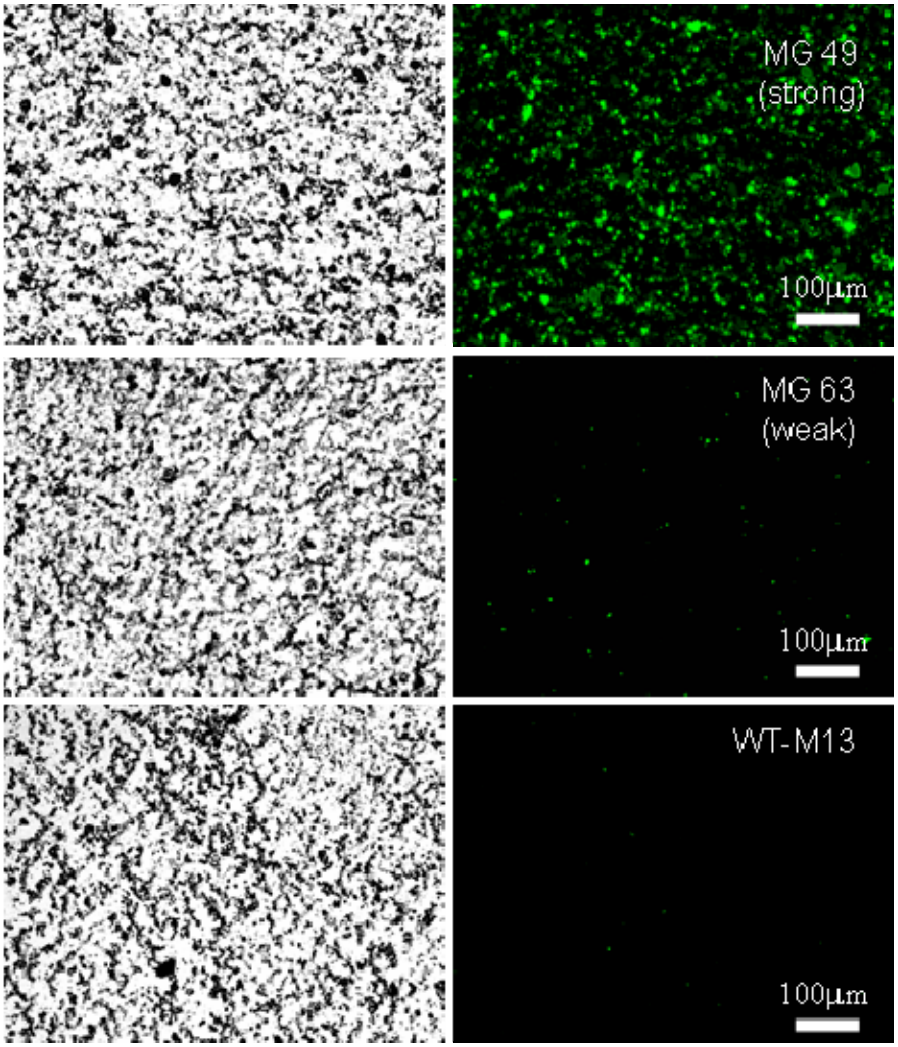


**Figure 3.1:** Bright field and fluorescent images of MG-49, MG-63 and wt - M13

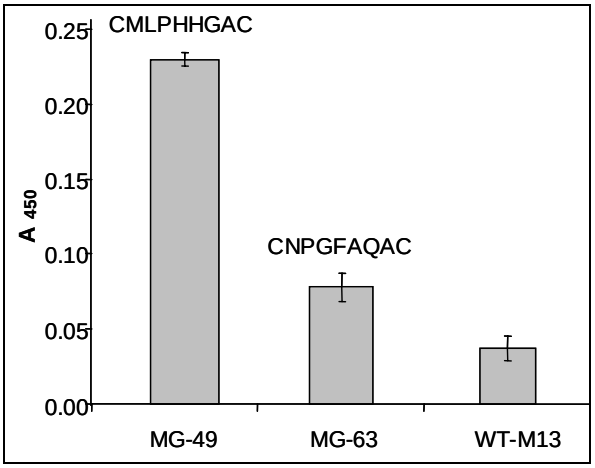


**Figure 3.2:** Relative binding affinities of MG-49, MG-63 and WT-M13 to hydroxyapatite determined by ELISA.

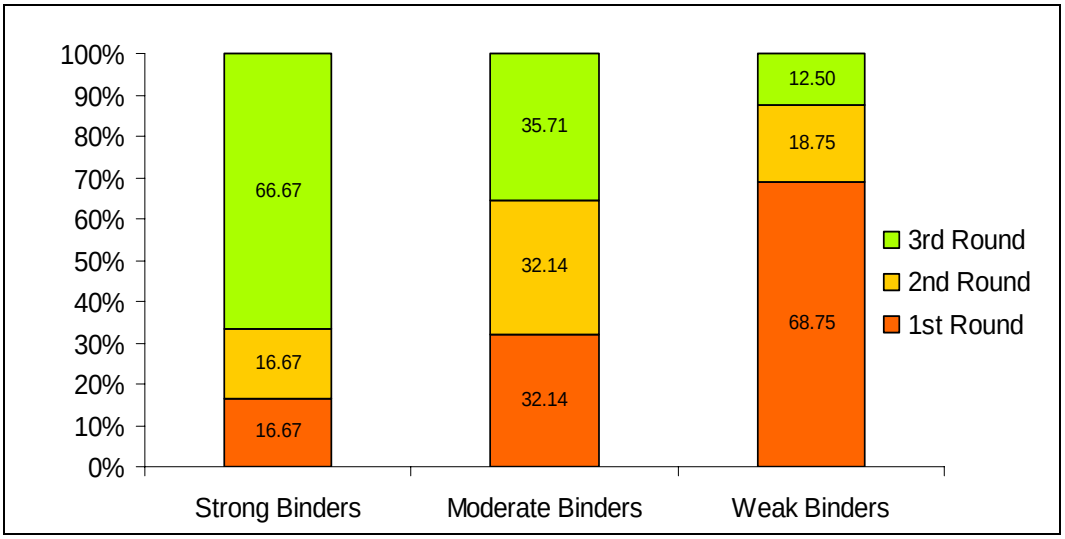


**Figure 3.3:** Percent distribution of strong, moderate and weak binders obtained from each round

### 3.2.2. Statistical Analysis of Amino Acids

Distribution of amino acids throughout the selected peptides was determined by calculating the occurrence percentage of amino acids. However, since distribution of amino acids are not the same in the library, relative abundances of amino acids were calculated by comparing the occurrence of amino acids in the library and in the selected binders. The calculation was made by dividing the difference between the distribution of an amino acid in the binder set and in the library to the distribution in the library. ([distribution in the binder set – distribution in the library] / distribution in the library) Relative abundances of amino acids among all sequences are shown in Figure 3.1. , Figure 3.2., Figure 3.3. and Figure 3.4.

Relative abundance calculations showed that Asp, Gln, His and Phe were over-expressed among all sequences. Relative abundances among strong, moderate and weak binders were also similar except for that Asn was over-expressed only among strong binders.

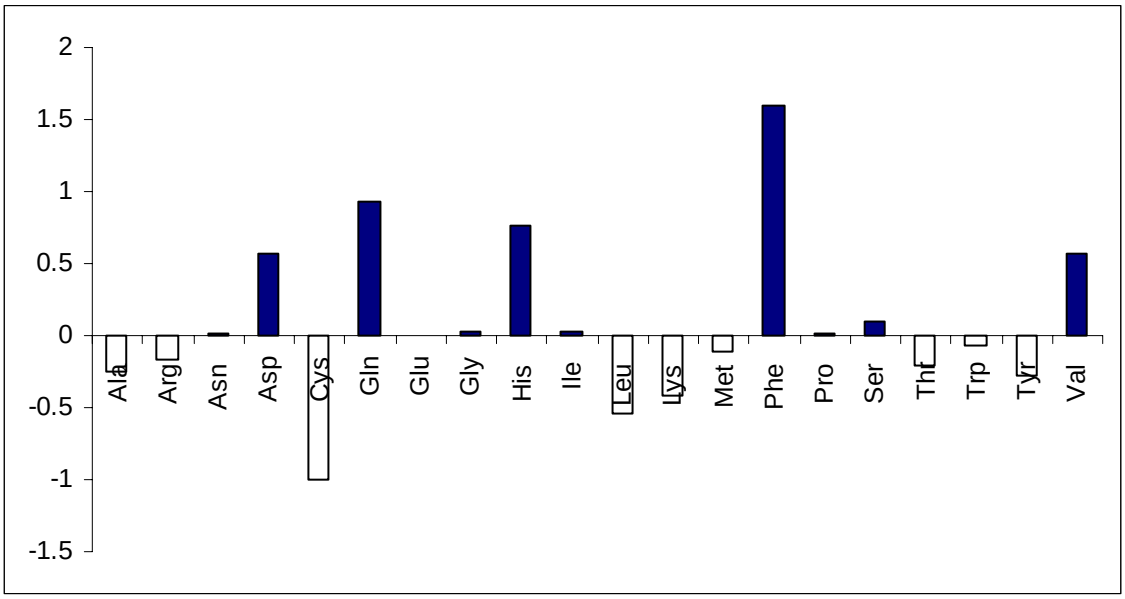


**Figure 3.4:** Relative abundance of amino acids among all selected sequences.

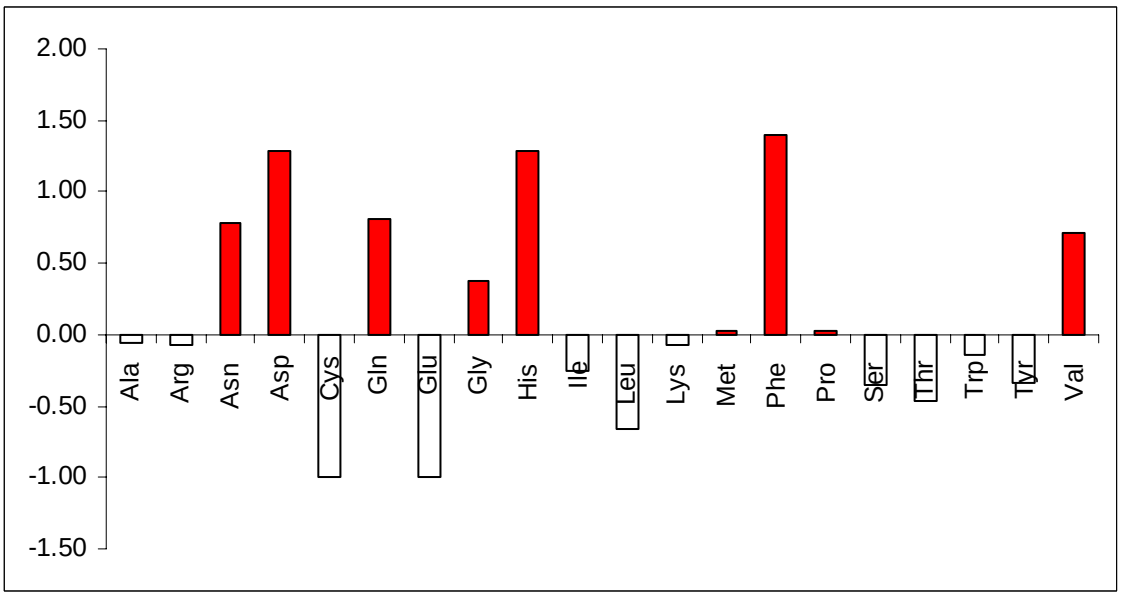


**Figure 3.5:** Relative abundance of amino acids among strong binders.

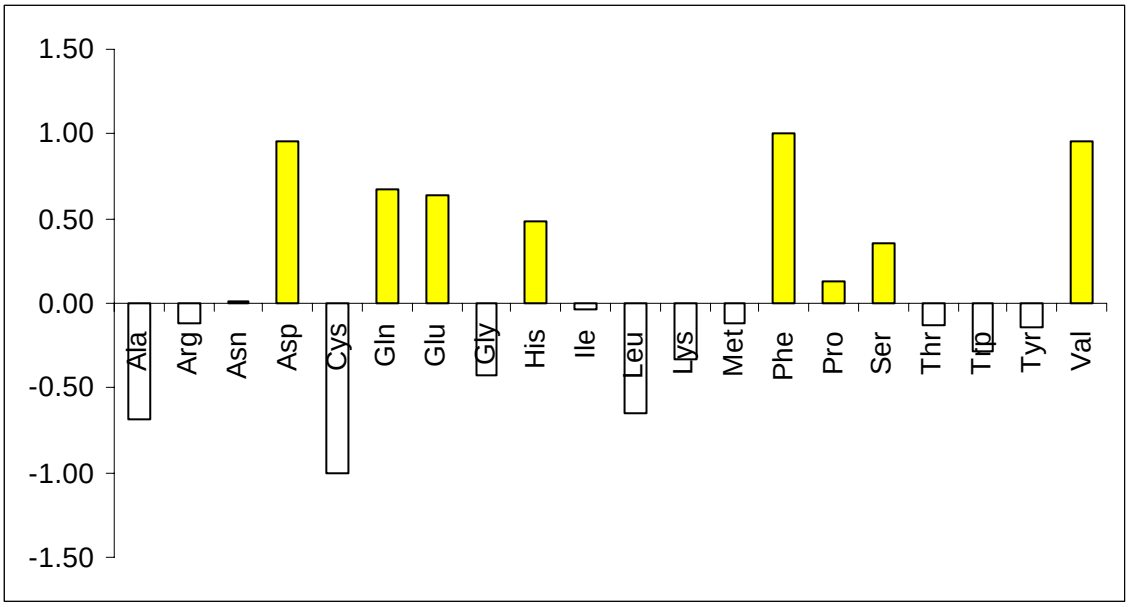


**Figure 3.6:** Relative abundance of amino acids among moderate binders.

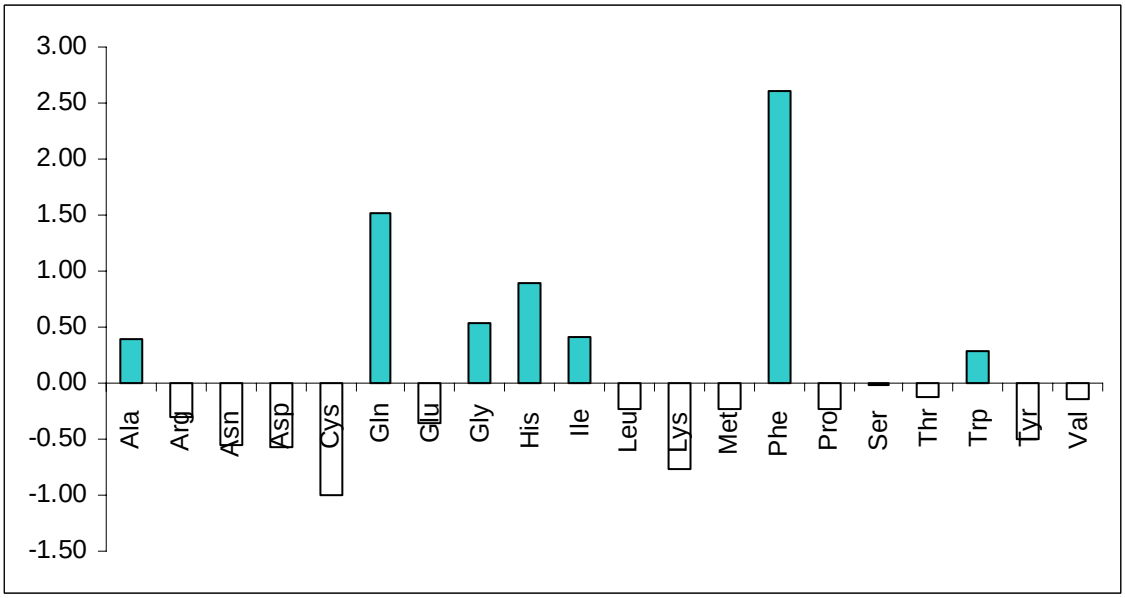


**Figure 3.7:** Relative abundance of amino acids among weak binders.

### 3.2.3. Physicochemical Analysis

Isoelectric point (pI) and molecular weight (MW) of the selected sequences was calculated by ExPasy ProtParam tool. (http://www.expasy.org/tools/protparam.html). Net charges of the peptides were calculated by subtracting the number of basic residues (Asp + Glu) from the number of acidic residues (Arg + Lys). The physicochemical properties of the strong, moderate and weak binding sequences are listed on Table 3.1., Table 3.2. and Table 3.3.

Physicochemical analysis revealed that most of the strong binders were carrying at least 1 charged amino acid while the number of sequences containing charged amino acids in weak binders were much less. (Figure 3.7.) This is an important distinction since acidic proteins, that are known to bind to hydroxyapatite and influence biomineralization, are known to carry polar side chains.

**Table 3.1:** Approximate surface coverage and physicochemical properties of moderate binders

| | Sequence | % Binding | MW | pI | Charge |
|---|---|---|---|---|---|
| MG61 | TPPHHQP | 40% | 812.9 | 6.61 | 0 |
| MG48 | HSPSNPS | 55% | 724.7 | 6.74 | 0 |
| MG101 | MHPTHTT | 38% | 823.9 | 6.69 | 0 |
| MG108 | HPATIED | 38% | 781.8 | 4.64 | -2 |
| MG107 | SGQISLL | 36% | 716.8 | 5.24 | 0 |
| MG55 | SGSPVPN | 33% | 656.6 | 5.24 | 0 |
| MG102 | DNTSDMV | 33% | 780.8 | 3.56 | -2 |
| MG105 | SSWQRLR | 31% | 932 | 12 | +2 |
| MG106 | QNKDFQK | 31% | 906.9 | 8.59 | +1 |
| MG65 | HQESHPP | 30% | 830.8 | 5.98 | -1 |
| MG62 | PHHHHQP | 29% | 888.9 | 7.49 | 0 |
| MG110 | SNYFAEM | 29% | 860.9 | 4 | -1 |
| MG117 | QSSHSFL | 29% | 804.8 | 6.74 | 0 |
| MG116 | AINDTNQ | 27% | 774.7 | 3.8 | -1 |
| MG68 | PTTPNEQ | 24% | 758.8 | 4 | -1 |
| MG30 | SMKVPSS | 22% | 734.8 | 8.47 | +1 |
| MG54 | SVEERGS | 22% | 762.7 | 4.53 | -1 |
| MG33 | NESFTGA | 22% | 724.7 | 4 | -1 |
| MG41 | YPTQTTD | 21% | 824.8 | 4.3 | -1 |
| MG42 | IYEVNTE | 21% | 866.9 | 4.24 | -2 |
| MG13 | SPQTPSR | 20% | 771.8 | 9.47 | +1 |
| MG47 | SDNTVRY | 19% | 853.8 | 5.55 | 0 |
| MG27 | SMIPPYR | 18% | 863 | 8.46 | +1 |
| MG45 | VLTPTQS | 18% | 744.8 | 5.49 | 0 |
| MG60 | RPIVHHQ | 16% | 886 | 9.76 | +1 |
| MG28 | MWRDSKP | 16% | 919 | 8.5 | +1 |
| MG103 | LSPKPQL | 9% | 781.9 | 8.75 | +1 |
| MG12 | YPPRSNT | 1% | 833.9 | 8.75 | +1 |

**Table 3.2:** Approximate surface coverage and physicochemical properties of strong binders

| | Sequence | % Binding | MW | pI | Charge |
|---|---|---|---|---|---|
| MG49 | MLPHHGA | 75% | 761.9 | 6.69 | 0 |
| MG31 | TTTPNRA | 70% | 759.8 | 9.41 | +1 |
| MG39 | PVAMPHW | 68% | 837 | 7.17 | 0 |
| MG100 | NNNYSRH | 68% | 903 | 8.75 | +1 |
| MG69 | PKDAVPA | 66% | 698.8 | 6.26 | 0 |
| MG29 | PSFDNGF | 64% | 782.8 | 3.8 | -1 |
| MG46 | QLIPVSN | 61% | 769.9 | 5.52 | 0 |
| MG52 | LTQSDHP | 58% | 769.8 | 5.08 | -1 |
| MG16 | HQHNMKI | 40% | 907 | 8.76 | +1 |
| MG32 | RTNQPQK | 52% | 870.9 | 11 | 2 |
| MG67 | DPQYGQH | 47% | 843.8 | 5.08 | -1 |
| MG10 | NSGSRHH | 46% | 793.8 | 9.76 | +1 |

**Table 3.3:** Approximate surface coverage and physicochemical properties of weak binders

| | Sequence | % Binding | MW | pI | Charge |
|---|---|---|---|---|---|
| MG15 | HQTHHPQ | 15% | 883.9 | 7.02 | 0 |
| MG63 | NPGFAQA | 8% | 703.7 | 5.52 | 0 |
| MG64 | GIGQPQA | 8% | 669.7 | 5.52 | 0 |
| MG19 | MIFLRVV | 6% | 877.1 | 9.5 | 1 |
| MG104 | TAHAMLY | 6% | 805.9 | 6.4 | 0 |
| MG109 | HLPIPSA | 6% | 733.8 | 6.74 | 0 |
| MG20 | MGAGRAA | 5% | 632.7 | 9.5 | 1 |
| MG34 | SIHSRDT | 4% | 814.8 | 6.46 | 0 |
| MG36 | TFHKWPS | 3% | 902 | 8.44 | 1 |
| MG50 | STWIPEF | 2% | 878.9 | 4 | -1 |
| MG51 | PSSPLQS | 2% | 714.7 | 5.96 | 0 |
| MG58 | HLHQQNT | 2% | 876.9 | 6.92 | 0 |
| MG59 | QLQLLQS | 1% | 828.9 | 5.52 | 0 |
| MG66 | RTTPSYH | 1% | 860.9 | 8.75 | 1 |
| MG118 | TTHQEAP | 1% | 782.8 | 5.21 | -1 |
| MG11 | TGLQNSS | 1% | 705.7 | 5.19 | 0 |

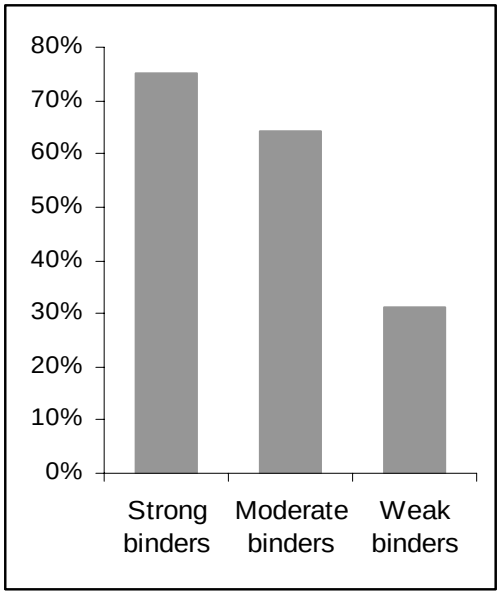


**Figure 3.8:** Percentage of peptides containing at least 1 charged amino acid among strong, moderate and weak binders.

### 3.3. *in vitro* Mineralization

At the end of the binding characterization, the strongest binding clone, MG-49 (CMLPHHGAC), with a surface coverage of 75%, and a weak binding clone, MG-63 (CNPFFAQAC), with a surface coverage of 4% and similar chemical properties with MG-49 clone were selected for *in vitro* mineralization experiments.

AP activity measurements were done prior to mineralization experiments. Activity measurements revealed no significant change between the AP activity in the presence of peptides and no peptide, indicating that the effects were due to the presence of the peptides. Activity of AP in the presence of no peptide, MG-49 and MG-63 is shown in Figure 3.8.

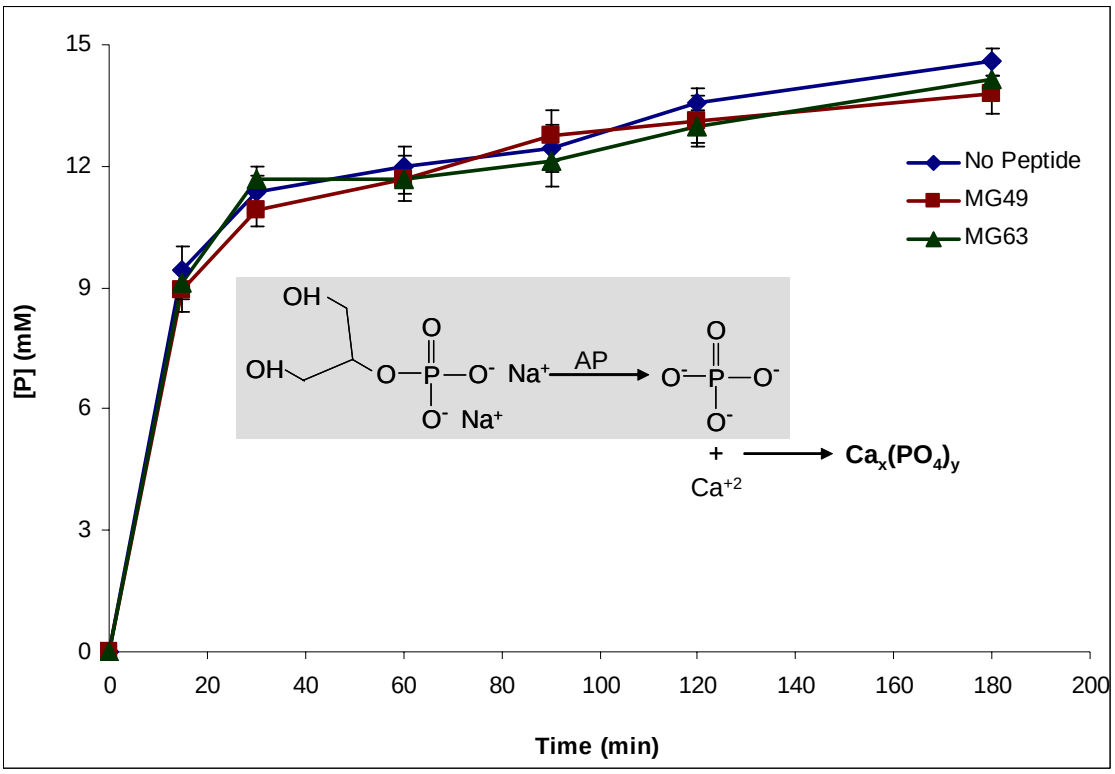


**Figure 3.9:** Phosphate concentrations released by AP in the presence of no peptide, MG-49 and MG-63 peptide.

### 3.3.1. Effect of Hydroxyapatite Binding Phages on *in vitro* Mineralization – Absorbance Measurements

Absorbance measurements revealed no significant difference between the absorbance increases in the presence of no phage and binder phages. The onset of the absorbance increase was observed around 15-20 minutes in all cases. At the end of the 1$^{st}$ hour, no significant difference was observed in the increase of the absorbance. (Figure 3.9.)

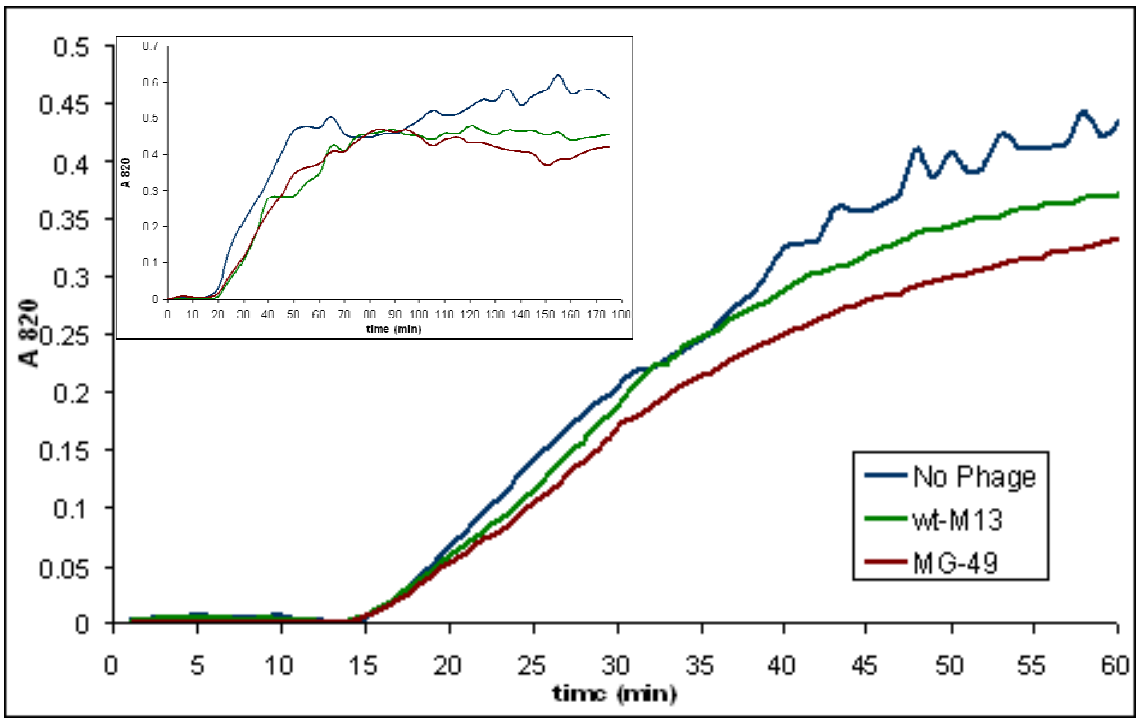


**Figure 3.10:** Effect of MG-49 and wt-M13 phage on mineralization measured by continuous absorbance measurements by multiplate reader. (inset: 0-180 minutes)

### 3.3.2. Effect of Hydroxyapatite Binding Phages on *in vitro* Mineralization – SEM Analysis

SEM analysis revealed no significant difference in the morphology of the formed minerals. Plate-like minerals were formed at the end of 10 days of mineralization in each case. The plate-like features formed in the presence of wild type M13 and MG-49 phage were slightly smaller than the ones formed in the presence of no phage. However, no morphological difference between the minerals formed in the presence of wild type M13 and MG-49 phage was observed (Figure 3.10.).

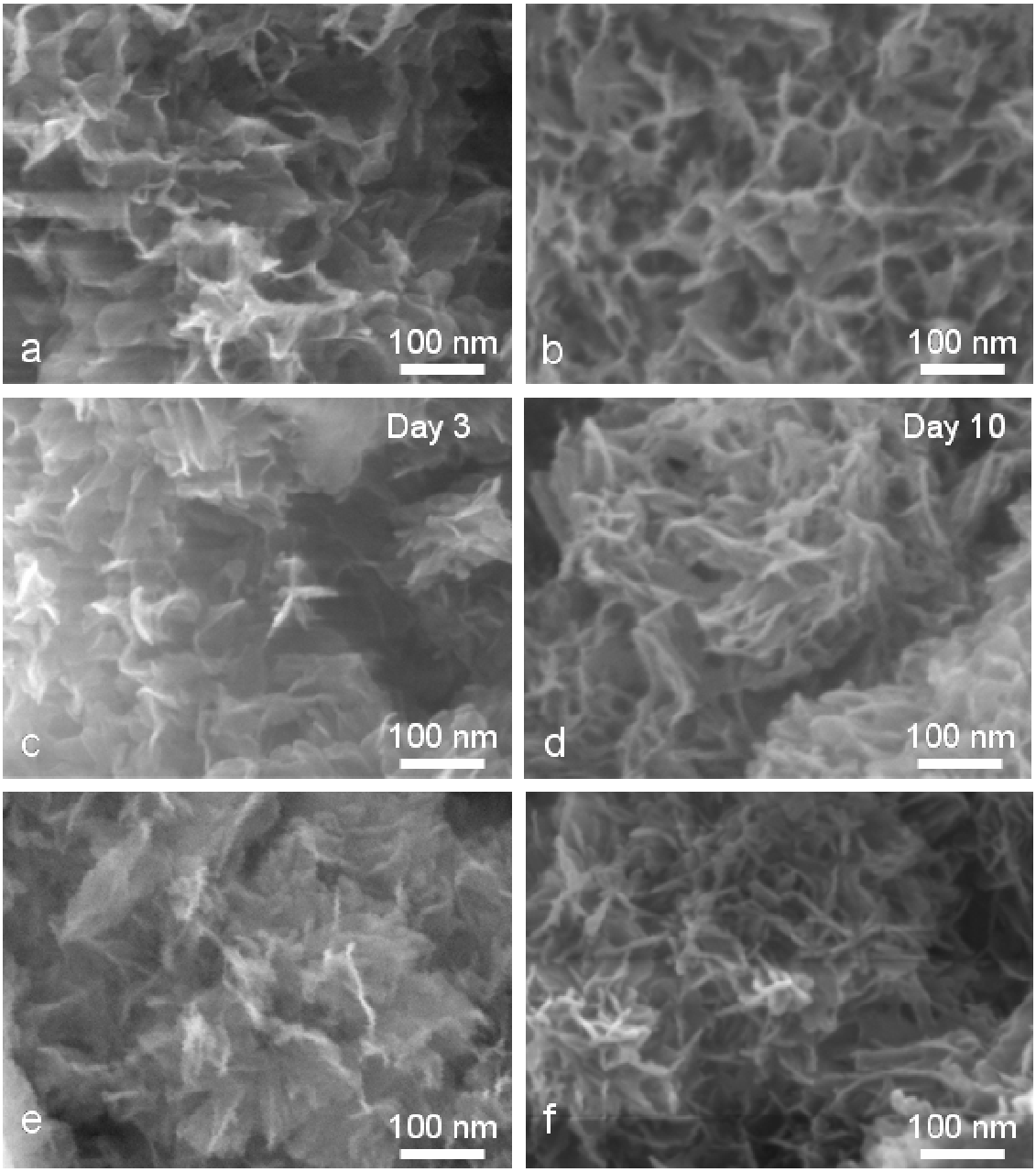


**Figure 3.11**. SEM images of the minerals formed in the presence of no phage (a-b), wild type M13 phage (c-d) and MG - 49 phage (e-f) at the end of 3 days and 10 days.

The possible reason for observing no morphological and kinetic difference in the presence of hydroxyapatite phages may be due to the size difference of the phage coat proteins and the displayed peptides. Since the size of the displayed peptide is much smaller than the coat proteins of M13 phage, the coat proteins may be blocking the effect of the displayed peptide even though they do not bind to the hydroxyapatite surface. Therefore, instead of using the phages to see the effects of the binding peptides, we commercially synthesized the peptide sequence displayed on the phage and used directly the peptides in the mineralization experiments.

### 3.3.3. Effect of Hydroxyapatite Binding Peptides on *in vitro* Mineralization – Absorbance Measurements

The mineralization in the presence of binding peptides was characterized via absorbance measurements, Ca-P measurements, SEM and TEM.

Absorbance measurements showed that the mineralization was effected by the presence of the peptides. In the presence of no peptide, the onset of the absorbance increase started at about 10 -15 minutes. In the presence of low concentration of both strong and weak binding peptides (0.07 mM), the onset of the absorbance was slightly delayed to 15-20 minutes and the increase in the absorbance was slightly reduced. There was no significant difference between the effect of the MG-49 and MG-63. However at high concentration of peptides (0.4 mM), a dramatic change was observed in the absorbance increase. In the case of MG-63, the onset of the absorbance was delayed significantly to 35-40 minutes and the absorbance was reduced about 1/3 at 90 minutes. The effect was more dramatic in the case of 0.4 mM MG-49. At the end of 90 minutes, there was almost no increase in the absorbance in the presence of MG-49. (Figure 3.12.a) The appearances of the reaction solutions were also consistent with the absorbance measurements. There was a fast increase in the turbidity of no peptide reaction. The reaction well of MG-49 reaction was still clear at the end of the 90 minutes. The retardation of the mineralization was to a lesser extent in the MG-63 reaction. At the end of 28 hours, turbidity of all reactions were similar, indicating that sufficient mineralization was occurred (Figure 3.12.b)

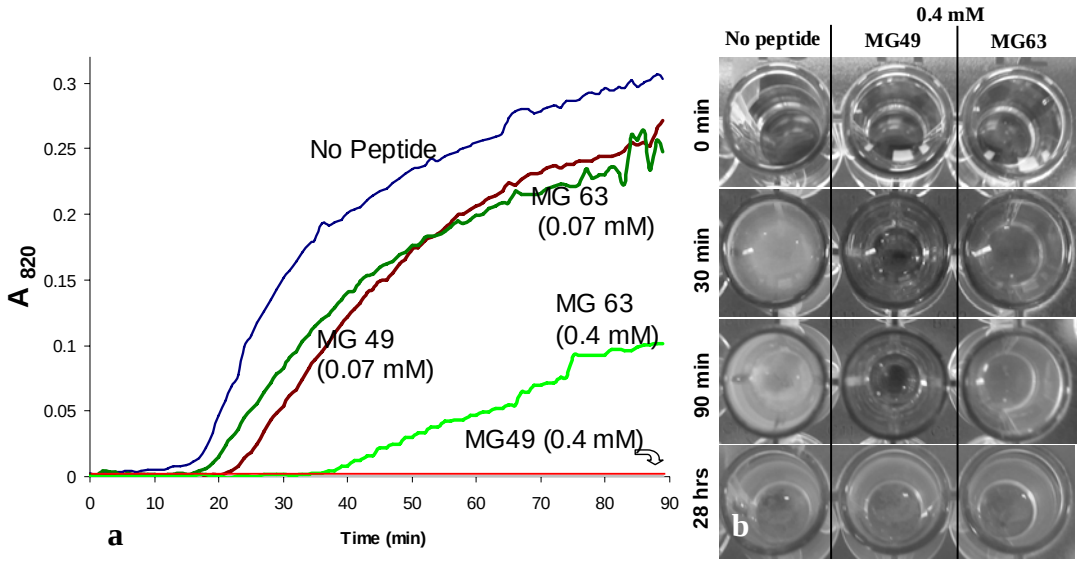


**Figure 3.12:** Effect of MG-63 and MG-49 on mineralization measured by **(a)** continuous absorbance measurements by multiplate reader and **(b)** optical images of the reaction solutions at different time points.

These initial findings indicate that the effects of the peptides are sequence and dose specific. However absorbance measurements give rough information about the reaction kinetics since it is not too sensitive. Therefore, reaction kinetics was further analyzed by calcium and phosphate measurements.

### 3.3.4. Effect of HABPs on *in vitro* Mineralization – Calcium and Phosphate Measurements

The effects of the peptides on mineralization kinetics were further investigated by measuring the used Ca and P amounts. The similar inhibition effect observed in absorbance measurements was observed with Ca and P measurements too. In the presence of no peptide, 75% of the Ca and 90% of the P were already consumed at the end of the first 6 hours. In the presence of MG-63, 63% of the Ca and 76% of the P was consumed at the end of 6 hours. However, in the presence of MG-49, only 25% of the Ca and 35% of the P was consumed in 6 hours. (Figure 3.13. b and d)

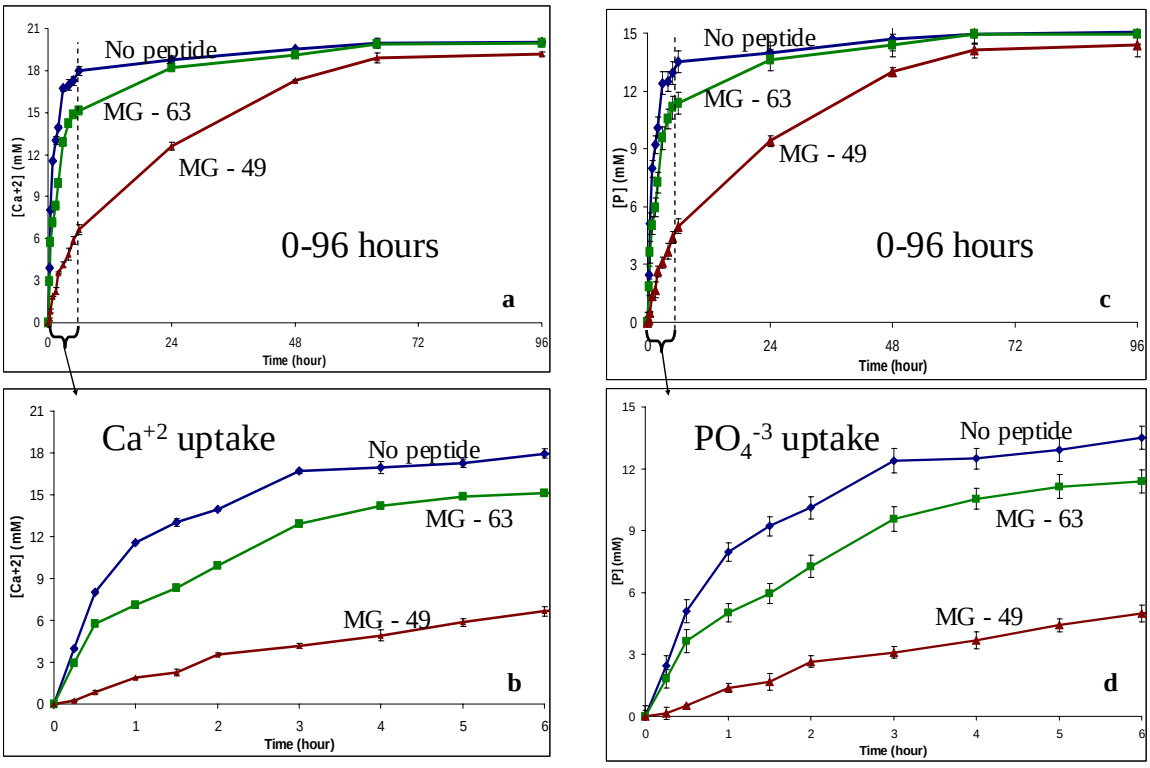


**Figure 3.13:** Concentrations of consumed Ca between **(a)** 0-96 hours **(b)** 0-6 hours and consumed P between **(c)** 0-96 hours and **(d)** 0-6 hours.

At the end of 96 hours, all of the Ca and P were used in no peptide and MG-63 reactions. However in MG-49 reactions about 1 mM Ca and P were not consumed. This may indicate that MG-49 may be inhibiting the mineralization by binding to the precursor molecules, Ca and P.

The reaction rates for the first 6 hours were calculated assuming 1st order kinetics using the calcium consumption rates. The reaction rates for no peptide, MG-63 and MG-49 were 7.9 x $10^{-3}$ / min, 3.9 x $10^{-3}$ / min, 1.2 x $10^{-3}$ / min, respectively. (Figure 3.14.) These results show that the mineralization reaction was inhibited about 1/2 in the presence of MG-63 and 1/4 in the presence of MG-49 compared to the reaction rate in the presence of no peptide.

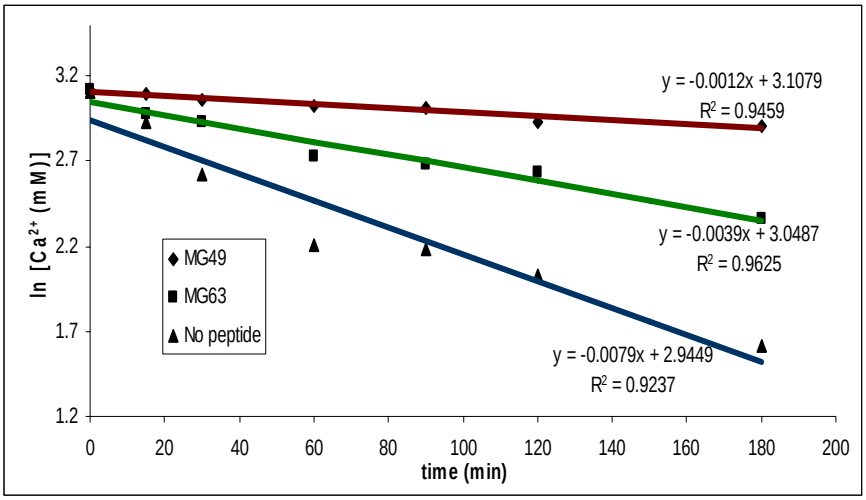


**Figure 3.14:** Reaction rates of mineralization assuming 1st order reaction kinetics based on $Ca^{+2}$ consumption.

Lastly, Ca / P ratios were calculated for no peptide, MG-63 and MG-49 reactions at given times. At the end of 30 minutes, the Ca / P ratio of all cases were about 1.55 – 1.6 which is the Ca / P ratio of the amorphous calcium phosphate (ACP, $Ca_9(PO_4)_6$). However, at the end of the 1st hour, Ca / P rate for no peptide and MG-63 was about 1.45 while the rate for MG-49 was about 1.37. At the end of 2.5 hour, the rate for MG-49 reaction reached to 1.33, which is the Ca / P ratio for octacalcium phosphate (OCP, $Ca_8H_2(PO_4)_6$), a precursor of hydroxyapatite, and stabilized for the rest of the reaction. However, no peptide and MG-63 reactions reached the same ratio at the end of the 4th hour before becoming stable for the rest of the reaction (Figure 3.16.). These results indicate that, the peptides not only affect the kinetics of the mineralization reaction, but also affect the conversion rate of the mineral from amorphous calcium - phosphate to crystalline calcium - phosphate.

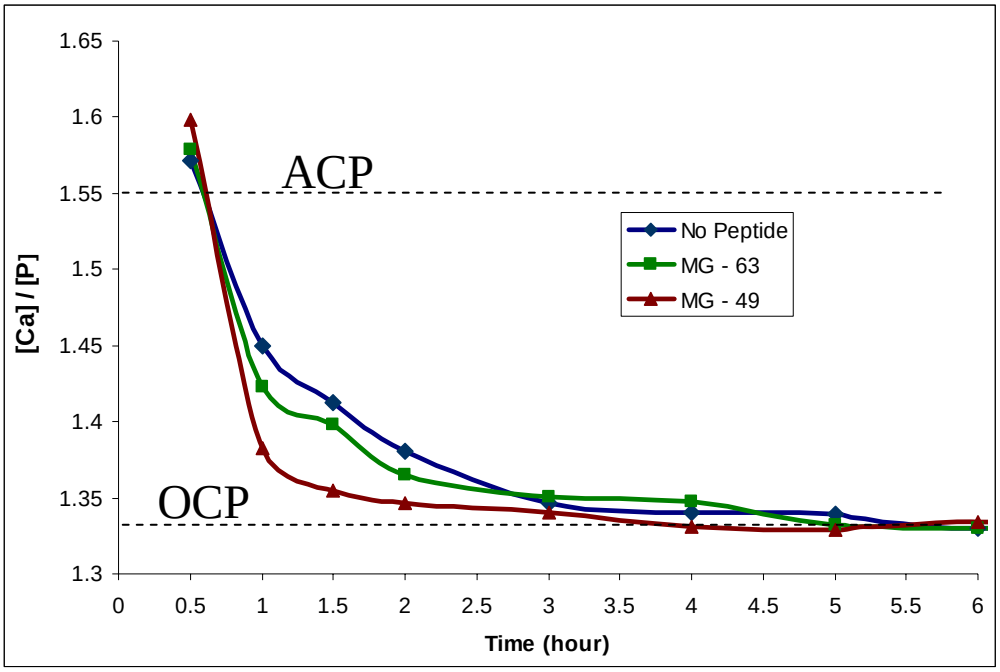


**Figure 3.15:** Ca / P ratio of the mineral formed in the presence of no peptide, MG-63 and MG-49

### 3.3.5. Effect of HABPs on *in vitro* Mineralization – TEM Analysis

The mineralized phase in all three cases was OCP as determined by electron diffraction analysis. TEM analysis showed that at the end of 96 hours, the size of the crystals formed in the presence of MG-49 was much bigger (Figure 3.16 a-b) than that of formed in the presence of MG-63 (Figure 3.16 c-d) and no peptide (Figure 3.16 e-f). As seen on Figure 3.16.e, the sizes of the crystals formed in the presence of MG-49 were not homogenous. The small crystals observed in no peptide and MG-63 cases were observed together with much larger crystals, larger crystals being dominant, for MG-49 case. Also in the presence of MG-63, slightly bigger crystals were observed compared to no peptide reaction, however, the size difference was not as dramatic as MG-49 case when compared to no peptide and the number of smaller crystals was dominant throughout the collected samples.

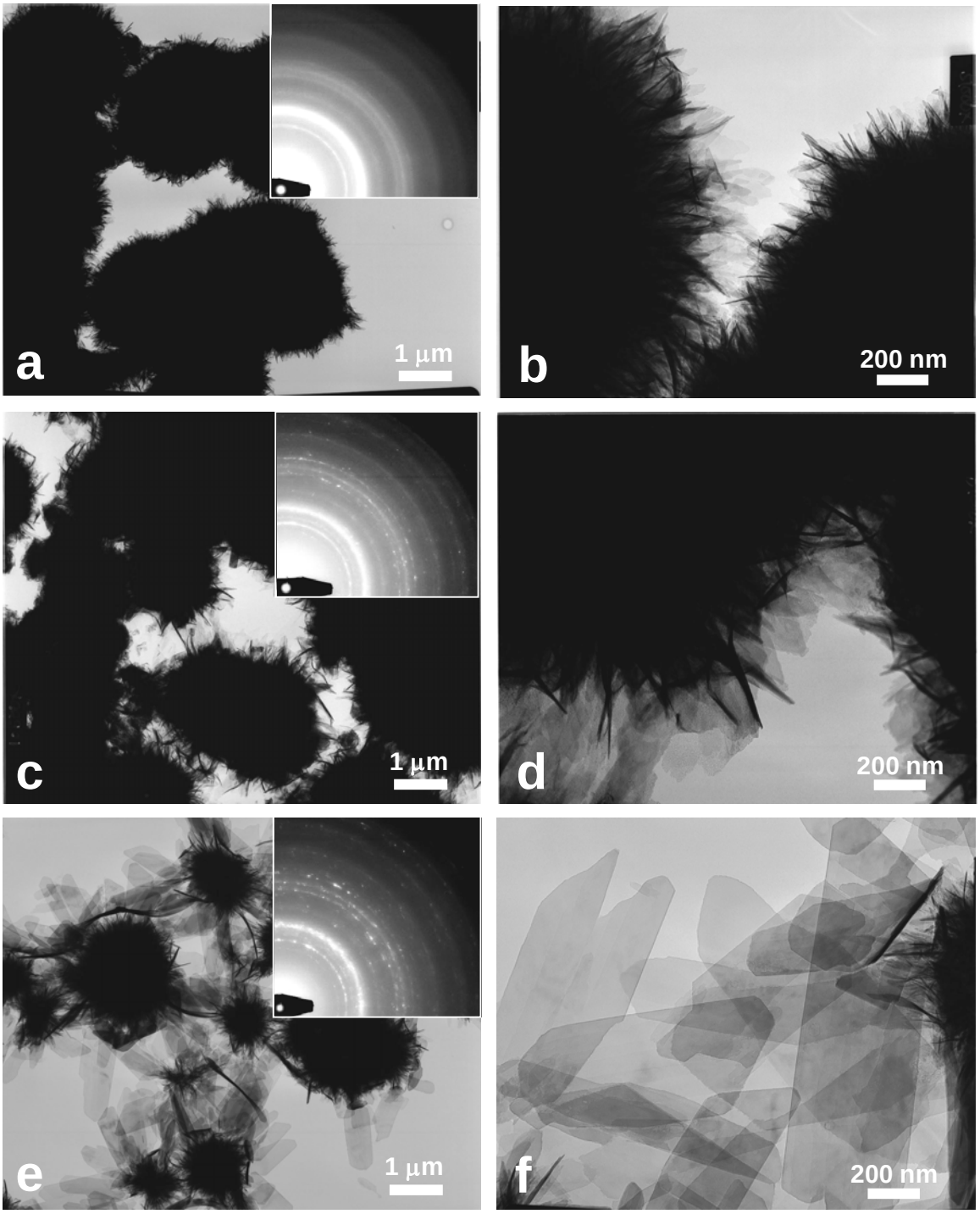


**Figure 3.16:** TEM images of the minerals formed in the presence of no peptide (a-b), MG-63 (b-c) and MG -49 (c-d) at the end of 96 hours. The insets in a, c and e are the selected area diffraction patterns for the shown minerals.

### 3.3.6. Effect of HABPs on *in vitro* Mineralization – SEM Analysis

A time wise analysis of morphology was made by SEM. At 30 minutes, globular particles were observed in both control and MG-49 reactions (Figure 3.17. a-b). However the size of the particles formed in the presence of MG-49 (~100 nm) was ~5 times smaller than that of formed in the presence of no peptide (~500nm). Also

the number of the particles formed in the presence of MG-49 was much less than that of formed in the presence of no peptide. At 90 minutes, the sizes of the globular features were grown to a similar size in both reactions (~ 1 μm). However, spicular features were observed on the particles formed in the presence of MG-49 while the particles formed in the presence of no peptides were still smooth. (Figure 3.17. c-d). At 2.5 hours, the size of the globular particles formed in the presence of no peptide did not change and spicular features appeared on them too. However no more globular particles were observed in MG-49 reaction due to the growth of the spicular features into plates. (Figure 3.17. e-f). At 28 hours, no change was observed in the morphology of the particles formed in the presence of no peptide, while the plates formed in the presence of MG-49 grew bigger. (Figure 3.17. g-h). No more morphological changes were observed in both reactions after 28 hours (not shown).

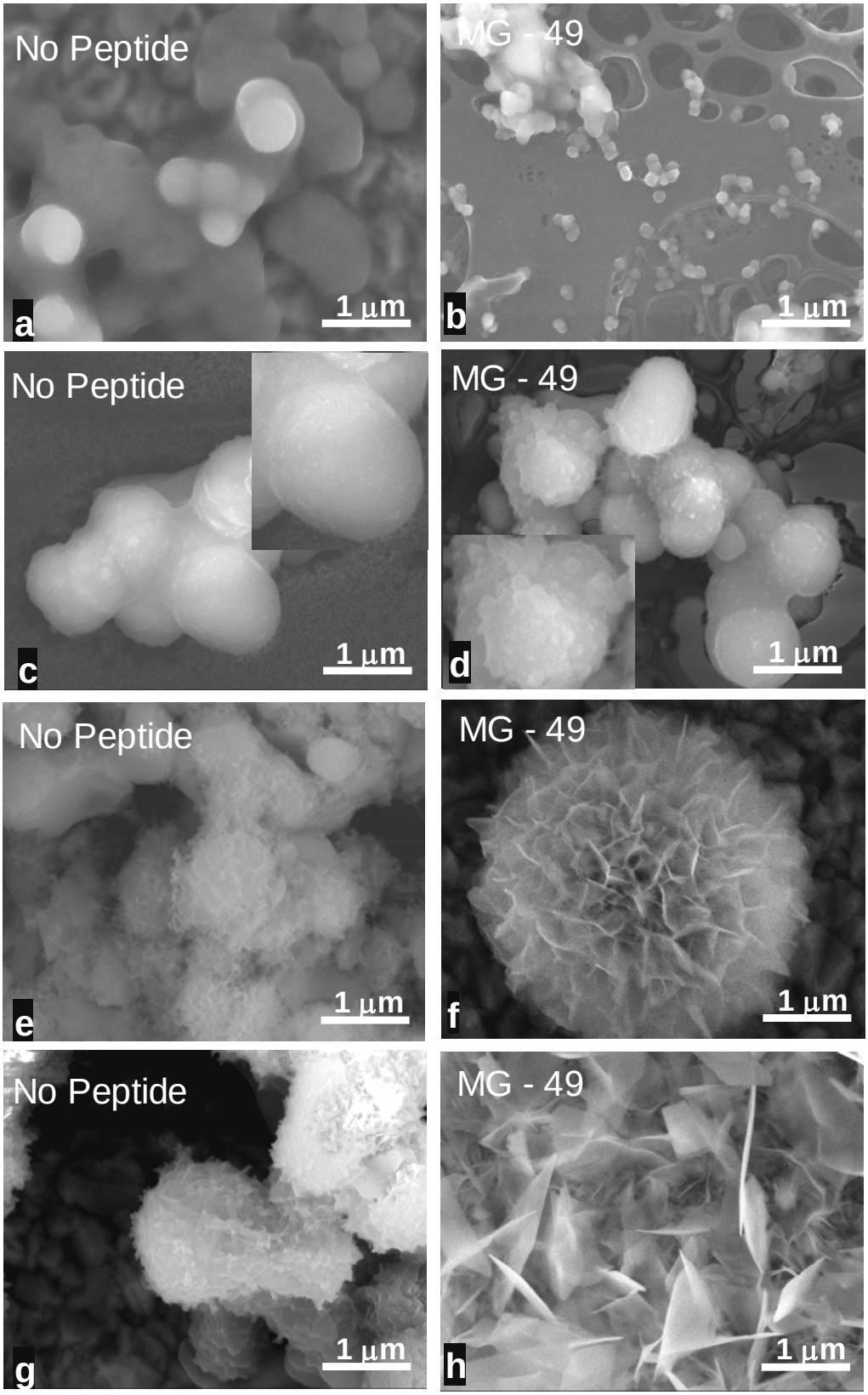


**Figure 3.17:** SEM images of the minerals formed in the presence of no peptide and MG- 49 collected at 0.5 hour (a-b), 1.5 hours (c-d), 2.5 hours (e-f) and 28 hours (g-h).

### 3.4. Effect Mechanisms of HABPs on *in vitro* Mineralization

The results obtained in this study demonstrate that combinatorially selected novel hydroxyapatite-binding peptides can significantly influence mineral formation and growth *in vitro*. The effect of the strong binding peptide selected for this study, MG-49, appears to be expressed during both the initial phase and the later stages of the mineralization. The reduction in the mineral formation and size at the initial stage of the mineralization (Figure 3.17. a-b) may indicate a nucleation inhibition due to chelation of $Ca^{+2}$ or $PO_4^{-3}$ ions by MG-49 peptide, therefore inhibiting the solution access of $Ca^{+2}$ or $PO_4^{-3}$. The $Ca^{+2}$ and $PO_4^{-3}$ measurements revealed that at the end of the $6^{th}$ our, 75% of the $Ca^{+2}$ and 90% of the $PO_4^{-3}$ were already consumed in the presence of no peptide while only 25% of the $Ca^{+2}$ and 35% of the $PO_4^{-3}$ was consumed in the presence of MG-49. (Figure 3.13. b-d). Therefore, almost all of the precursors were consumed in the presence of no peptide resulting in crystals with high in the number but small in the size. On the other hand, at the same time point, there were still enough amounts of precursors for the growth of formed mineral in the presence of MG-49 resulting in crystals with low in the number but large in the size.

Again the $Ca^{+2}$ and $PO_4^{-3}$ measurements showed that all of the $Ca^{+2}$ and $PO_4^{-3}$ were consumed at the end of 96 hours (Figure 3.13. a-c). This may be due to binding of the peptide to the crystal surface instead of the $Ca^{+2}$ or $PO_4^{-3}$ ions resulting in the release of the $Ca^{+2}$ or $PO_4^{-3}$ ions bound to the peptide as the mineralization proceeds. Since the selected have affinity to hydroxyapatite powder, one would expect the peptide to have less free energy when bound to the mineral surface; therefore, prefer to bind to the crystal surface instead of the $Ca^{+2}$ or $PO_4^{-3}$ ions as the mineralization proceeds.

TEM and SEM observations of the minerals obtained from MG-49 reaction showed that minerals bearing similar morphological characteristics to those obtained from control and MG-63 reactions co-exist with large crystals formed only in MG-49 reaction. These findings are due to that nucleation and growth processes occur at the same time during the process. As $PO_4^{-3}$ is released by AP it is consumed for both growth of already formed nuclei and formation of new nuclei. Therefore, at the end of the reaction, when there are no more precursors left for mineralization, we observe large crystals and smaller crystals which couldn't grow.

## REFERENCES


**Afshar, A., Ghorbani, M., Ehsani, N., Saeri, M. R., and Sorrell, C. C.** 2003. Some important factors in the wet precipitation process of hydroxyapatite. *Materials and Design* 24 **3**:197-202.

**Ball, P.** 2001. Life's lessons in design. *Nature* 409 **6818**:413-416.

**Bellows, C. G., Aubin, J. E. and Heersche, J. N. M.** 1991. Initiation And Progression Of Mineralization Of Bone Nodules Formed Invitro - The Role Of Alkaline-Phosphatase And Organic Phosphate. *Bone And Mineral* 14 **1**:27-40.

**Beniash, E., Simmer, J. P., and Margolis, H. C.** 2005. The effect of recombinant mouse amelogenins on the formation and organization of hydroxyapatite crystals in vitro. *Journal Of Structural Biology* 149 **2**:182-190.

**Blakemore, R.** 1975. Magnetotactic Bacteria. *Science* 190 **4212**:377-379.

**Brown, S.** 1992. Engineered Iron Oxide-Adhesion Mutants Of The Escherichia-Coli Phage-Lambda Receptor. *Proceedings Of The National Academy Of Sciences Of The United States Of America* 89 **18**:8651-8655.

**Cariolou, M. A., and Morse, D. E.** 1988. Purification And Characterization Of Calcium-Binding Conchiolin Shell Peptides From The Mollusk, Haliotis-Rufescens, As A Function Of Development. *Journal Of Comparative Physiology B-Biochemical Systemic And Environmental Physiology* 157 **6**:717-729.

**Chen, B., Blair, D. G., Plisov, S., Vasiliev, G. A. Perantoni, O., Athanasiou, Q. M., Wu, J. Y., Oppenheim, J. J. and Yang, D.** 2004. Cutting edge: Bone morphogenetic protein antagonists Drm/Gremlin and Dan interact with slits and act as negative regulators of monocyte chemotaxis. *Journal Of Immunology* 173 **10**:5914-5917.

**Clezardin, P., Trzeciak, C. M. M. C., Drouin, J., and Delmas, P. D.** 1991. Thrombospondin Binds To The Surface Of Human Osteosarcoma Cells And Mediates Platelet-Osteosarcoma Cell-Interaction. *Cancer Research* 51 **10**:2621-2627.

**Daculsi, G., Legeros, R. Z., Legeros, J. P. and Mitre, D.** 1991. Lattice-Defects In Calcium-Phosphate Ceramics - High-Resolution Tem Ultrastructural-Study. *Journal Of Applied Biomaterials* 2 **3**:147-152.

**Danner, S., and Belasco, J. G.** 2001. T7 phage display: A novel genetic selection system for cloning RNA-binding proteins from cDNA libraries. *Proceedings Of The National Academy Of Sciences Of The United States Of America* 98 **23**:12954-12959.

**Demaeyer, E. A. P., Verbeeck, R. M. H. and Naessens, D. E.** 1994. Effect Of Heating On The Constitution Of Na+-Containing And Co3(2-)-Containing

Apatites Obtained By The Hydrolysis Of Monetite. *Inorganic Chemistry* 33 **26**:5999-6006.

**Deptula, A., M. Carewska, T. Olczak, W. Lada, and F. Croce.** 1993. Sintering Of Zro2-Ceo2 Spherical Powders Prepared By A Water Extraction Variant Of The Sol-Gel Process. *Journal Of The Electrochemical Society* 140 **8**:2294-2297.

**Devries, I. G., and E. Wisse.** 1989. Ultrastructural-Localization Of Dentin Phosphoprotein In Rat Tooth Germs By Immunogold Staining. *Histochemistry* 91 **1**:69-75.

**Dickerson, M. B., R. R. Naik, M. O. Stone, Y. Cai, and K. H. Sandhage.** 2004. Identification of peptides that promote the rapid precipitation of germania nanoparticle networks via use of a peptide display library. *Chemical Communications* **15**:1776-1777.

**Dimuzio, M. T., and A. Veis.** 1978. Phosphophoryns - Major Non-Collagenous Proteins Of Rat Incisor Dentin. *Calcified Tissue Research* 25 **2**:169-178.

**Doi, Y., T. Horiguchi, S. H. Kim, Y. Moriwaki, N. Wakamatsu, M. Adachi, K. Ibaraki, K. Moriyama, S. Sasaki, and H. Shimokawa.** 1992. Effects Of Noncollagenous Proteins On The Formation Of Apatite In Calcium Beta-Glycerophosphate Solutions. *Archives Of Oral Biology* 37 **1**:15-21.

**Doi, Y., T. Horiguchi, S. H. Kim, Y. Moriwaki, N. Wakamatsu, M. Adachi, H. Shigeta, S. Sasaki, and H. Shimokawa.** 1993. Immobilized Dpp And Other Proteins Modify Ocp Formation. *Calcified Tissue International* 52 **2**:139-145.

**Donadel, K., M. C. M. Laranjeira, V. L. Goncalves, V. T. Favere, J. C. de Lima, and L. H. M. Prates.** 2005. Hydroxyapatites produced by wet-chemical methods. *Journal Of The American Ceramic Society* 88 **8**:2230-2235.

**Ducy, P., C. Desbois, B. Boyce, G. Pinero, B. Story, C. Dunstan, E. Smith, J. Bonadio, S. Goldstein, C. Gundberg, A. Bradley, and G. Karsenty.** 1996. Increased bone formation in osteocalcin-deficient mice. *Nature* 382 **6590**:448-452.

**Feng, W., and M. S. Li.** 2005. A biomimetic method of hydroxyapatite powders synthesized in simulated body fluid. *In Advances In Fracture And Strength*, Pts 1- 4.

**Ferry, D. and S.M. Goodnick.** 1997. Transport in nanostructures. Cambridge, U.K.: Cambridge University Press.

**Fincham, A. G., J. Moradian-Oldak, and J. P. Simmer.** 1999. The structural biology of the developing dental enamel matrix. *Journal Of Structural Biology* 126 **3**:270-299.

**Flores, M. E., M. Norgard, D. Heinegard, F. P. Reinholt, and G. Andersson.** 1992. Rgd-Directed Attachment Of Isolated Rat Osteoclasts To Osteopontin, Bone Sialoprotein, And Fibronectin. *Experimental Cell Research* 201 **2**:526-530.

**Fong, H., S. N. White, M. L. Paine, W. Luo, M. L. Snead, and M. Sarikaya.** 2003. Enamel structure properties controlled by engineered proteins in transgenic mice. *Journal Of Bone And Mineral Research* 18 **11**:2052-2059.

**Fuierer, T. A., M. Lore, S. A. Puckett, and G. H. Nancollas.** 1994. A Mineralization Adsorption And Mobility Study Of Hydroxyapatite Surfaces In The Presence Of Zinc And Magnesium Ions. *Langmuir* 10 **12**:4721-4725.

**Fujisawa, R., and Y. Kuboki.** 1991. Preferential Adsorption Of Dentin And Bone Acidic Proteins On The (100) Face Of Hydroxyapatite Crystals. *Biochimica Et Biophysica Acta* 1075 **1**:56-60.

**Fujisawa, R., and Kuboki, Y.,** 1992. Affinity Of Bone Sialoprotein And Several Other Bone And Dentin Acidic Proteins To Collagen Fibrils*. Calcified Tissue International* 51 **6**:438-442.

**Ganss, B., R. H. Kim, and J. Sodek.** 1999. Bone sialoprotein. *Critical Reviews In Oral Biology and Medicine* 10 **1**:79-98.

**Gibson, A. C., and K. E. Horak.** 1978. Systematic Anatomy And Phylogeny Of Mexican Columnar Cacti. *Annals Of The Missouri Botanical Garden* 65 **4**:999-1057.

**Gomez-Morales, J., J. Torrent-Burgues, T. Boix, J. Fraile, and R. Rodriguez-Clemente.** 2001. Precipitation of stoichiometric hydroxyapatite by a continuous method. *Crystal Research And Technology* 36 **1**:15-26.

**Gorski, J. P.** 1991. Calcium-Binding Properties Of Individual Extracellular Phosphoproteins From Bone. *Abstracts Of Papers Of The American Chemical Society* **201**:91-IEC.

**Harrison, G., I. M. Shapiro, and E. E. Golub.** 1995. The Phosphatidylinositol-Glycolipid Anchor On Alkaline-Phosphatase Facilitates Mineralization Initiation In-Vitro. *Journal Of Bone And Mineral Research* 10 **4**:568-573.

**He, G., T. Dahl, A. Veis, and A. George.** 2003. Nucleation of apatite crystals in vitro by self-assembled dentin matrix protein, 1. *Nature Materials* 2 **8**:552-558.

**Hoang, A. M., R. J. Klebe, B. Steffensen, O. H. Ryu, J. P. Simmer, and D. L. Cochran.** 2002. Amelogenin is a cell adhesion protein. *Journal Of Dental Research* 81 **7**:497-500.

**Hunter, G. K., P. V. Hauschka, A. R. Poole, L. C. Rosenberg, and H. A. Goldberg.** 1996. Nucleation and inhibition of hydroxyapatite formation by mineralized tissue proteins. *Biochemical Journal* **317**:59-64.

**Ibaraki, K., J. D. Termine, S. W. Whitson, and M. F. Young.** 1992. Bone-Matrix Messenger-Rna Expression In Differentiating Fetal Bovine Osteoblasts. *Journal Of Bone And Mineral Research* 7 **7**:743-754.

**Iijima, M., Y. Moriwaki, T. Takagi, and J. Moradian-Oldak.** 2001. Effects of bovine amelogenins on the crystal morphology of octacalcium phosphate in a model system of tooth enamel formation. *Journal Of Crystal Growth* 222 **3**:615-626.

**Johnsson, M., J. W. Perich, E. C. Reynolds, and G. H. Nancollas.** 1993. The Hydroxyapatite Binding Domains Of Statherin - Influence Of Size And Charge. *Journal Of Colloid And Interface Science* 160 **1**:179-182.

**Kao, K. Y. T., C. M. Vernier, and T. H. McGavack.** 1965. Connective Tissue .9. Metabolism Of Collagen In Bone Of Rat. *Proceedings Of The Society For Experimental Biology And Medicine* 119 **2**:584-and.

**Karlsson, F., C. A. K. Borrebaeck, N. Nilsson, and A. C. Malmborg-Hager.** 2003. The mechanism of bacterial infection by filamentous phages involves molecular interactions between TolA and phage protein 3 domains. *Journal Of Bacteriology* 185 **8**:2628-2634.

**Katz, E. P., and S. Li**. 1973. Structure And Function Of Bone Collagen Fibrils. *Journal Of Molecular Biology* 80 **1**:1-15.

**Kinney, J. H., S. Habelitz, S. J. Marshall, and G. W. Marshall.** 2003. The importance of intrafibrillar mineralization of collagen on the mechanical properties of dentin. *Journal Of Dental Research* 82 **12**:957-961.

**Knott, L., and A. J. Bailey.** 1998. Collagen cross-links in mineralizing tissues: A review of their chemistry, function, and clinical relevance. *Bone* 22 **3**:181-187.

**Koutsopoulos, S., and E. Dalas.** 2000. The effect of acidic amino acids on hydroxyapatite crystallization. *Journal Of Crystal Growth* 217 **4**:410-415.

**Layrolle, P., A. Ito, and T. Tateishi.** 1998. Sol-gel synthesis of amorphous calcium phosphate and sintering into microporous hydroxyapatite bioceramics. *Journal Of The American Ceramic Society* 81 **6**:1421-1428.

**Lee, S. W., C. B. Mao, C. E. Flynn, and A. M. Belcher.** 2002. Ordering of quantum dots using genetically engineered viruses. *Science* 296 **5569**:892-895.

**Lee, S. Y., J. H. Choi, and Z. H. Xu.** 2003. Microbial cell-surface display. *Trends In Biotechnology* 21 **1**:45-52.

**Lerner, E., S. Sarig, and R. Azoury.** 1991. Enhanced Maturation Of Hydroxyapatite From Aqueous-Solutions Using Microwave Irradiation. *Journal Of Materials Science-Materials In Medicine* 2 **3**:138-141.

**Lewin, J., and C. H. Chen.** 1968. Silicon Metabolism In Diatoms .6. Silicic Acid Uptake By A Colorless Marine Diatom Nitzschia Alba Lewin And Lewin. *Journal Of Phycology* 4 **2**:161-and.

**Li, C. M., G. D. Botsaris, and D. L. Kaplan.** 2002. Selective in vitro effect of peptides on calcium carbonate crystallization. *Crystal Growth and Design* 2 **5**:387-393.

**Liou, Y. C., A. Tocilj, P. L. Davies, and Z. C. Jia.** 2000. Mimicry of ice structure by surface hydroxyls and water of a beta-helix antifreeze protein. *Nature* 406 **6793**:322-324.

**Long, J. R., J. L. Dindot, H. Zebroski, S. Kiihne, R. H. Clark, A. A. Campbell, P. S. Stayton, and G. P. Drobny.** 1998. A peptide that inhibits hydroxyapatite growth is in an extended conformation on the crystal surface. *Proceedings Of The National Academy Of Sciences Of The United States Of America* 95 **21**:12083-12087.

**Lopez-Macipe, A., R. Rodriguez-Clemente, A. Hidalgo-Lopez, I. Arita, M. V. Garcia-Garduno, E. Rivera, and V. M. Castano.** 1998. Wet chemical synthesis of hydroxyapatite particles from nonstoichiometric solutions. *Journal Of Materials Synthesis And Processing* 6 **1**:21-26.

**Luo, G. B., P. Ducy, M. D. McKee, G. J. Pinero, E. Loyer, R. R. Behringer, and G. Karsenty.** 1997. Spontaneous calcification of arteries and cartilage in mice lacking matrix GLA protein. *Nature* 386 **6620**:78-81.

**Luo, P., and T. G. Nieh.** 1995. Synthesis of ultrafine hydroxyapatite particles by a spray dry method. *Materials Science and Engineering C-Biomimetic Materials Sensors And Systems* 3 **2**:75-78.

**Mann S, ed.** 1996. Biomimetic Materials Chemistry. New York: VCH

**Manner, G., Kretsing.Rh, B. S. Gould, and A. Rich.** 1967. Polyribosomal Synthesis Of Collagen. *Biochimica Et Biophysica Acta* 134 **2**:411-and.

**Mann, S., D. D. Archibald, J. M. Didymus, T. Douglas, B. R. Heywood, F. C. Meldrum, and N. J. Reeves.** 1993. Crystallization At Inorganic-Organic Interfaces - Biominerals And Biomimetic Synthesis. *Science* 261 **5126**:1286-1292.

**Mayer, G., and M. Sarikaya.** 2002. Rigid biological composite materials: Structural examples for biomimetic design. *Experimental Mechanics* 42 **4**:395-403.

**Mayer, U., M. Aumailley, K. Mann, R. Timpl, and J. Engel.** 1991. Calcium-Dependent Binding Of Basement-Membrane Protein Bm-40 (Osteonectin, Sparc) To Basement-Membrane Collagen Type-Iv. *European Journal Of Biochemistry* 198 **1**:141-150.

**McKee, M. D., and A. Nanci.** 1996. Osteopontin deposition in remodeling bone: An osteoblast mediated event. *Journal Of Bone And Mineral Research* 11 **6**:873-874.

**Mengeot, M., M. L. Harvill, and O. R. Gilliam.** 1973. Hydrothermal Growth Of Calcium Hydroxyapatite Single-Crystals. *Journal of Crystal Growth* 19 **3**:199-203.

**Moreno, E. C., K. Varughese, and D. I. Hay.** 1979. Effect Of Human Salivary Proteins On The Precipitation Kinetics Of Calcium-Phosphate. *Calcified Tissue International* 28 **1**:7-16.

**Murugan, R., K. P. Rao, and T. S. S. Kumar.** 2003. Microwave synthesis of bioresorbable carbonated hydroxyapatite using goniopora. *In Bioceramics* 15.

**Naik, R. R., L. L. Brott, S. J. Clarson, and M. O. Stone.** 2002. Silica-precipitating peptides isolated from a combinatorial phage display peptide library. *Journal Of Nanoscience And Nanotechnology* 2 **1**:95-100.

**Naik, R. R., S. J. Stringer, G. Agarwal, S. E. Jones, and M. O. Stone.** 2002. Biomimetic synthesis and patterning of silver nanoparticles. *Nature Materials* 1 **3**:169-172.

**Niemeyer, C. M.** 2001. Nanoparticles, proteins, and nucleic acids: Biotechnology meets materials science. *Angewandte Chemie-International Edition* 40 **22**:4128-4158.

**Noren, K. A., and C. J. Noren.** 2001. Construction of high-complexity combinatorial phage display peptide libraries. *Methods* 23 **2**:169-178.

**Nygaard, S., R. Wendelbo, and S. Brown.** 2002. Surface-specific zeolite-binding proteins. *Advanced Materials* 14 **24**:1853-1856.

**Paine, M. L., and M. L. Snead.** 1996. Tuftelin self-assembles through interactions between the carboxyl-terminals. *Journal Of Dental Research* **75**:1442-1442.

**Paine, M. L., Krebsbach, P. H., Chen, L. S., Paine, C. T., Yamada, Y., Deutsch, D. and Snead, M. L,.** 1997. Protein interactions during assembly of the enamel organic extracellular matrix. *Journal Of Bone And Mineral Research* 12 **2**:221-227.

**Pelletier, J., and S. Sidhu.** 2001. Mapping protein-protein interactions with combinatorial biology methods. *Current Opinion In Biotechnology* 12 **4**:340-347.

**Price, P. A.** 1985. Vitamin-K-Dependent Formation Of Bone Gla Protein (Osteocalcin) And Its Function. *Vitamins And Hormones-Advances In Research And Applications* **42**:65-108.

**Raines, E. W., T. F. Lane, M. L. Iruelaarispe, R. Ross, and E. H. Sage.** 1992. The Extracellular Glycoprotein Sparc Interacts With Platelet-Derived Growth-Factor (Pdgf)-Ab And (Pdgf)-Bb And Inhibits The Binding Of Pdgf To Its Receptors. *Proceedings Of The National Academy Of Sciences Of The United States Of America* 89 **4**:1281-1285.

**Rao, R. R., H. N. Roopa, and T. S. Kannan.** 1997. Solid state synthesis and thermal stability of HAP and HAP - beta-TCP composite ceramic powders. *Journal Of Materials Science-Materials In Medicine* 8 **8**:511-518.

**Rhee, S. H.** 2002. Synthesis of hydroxyapatite via mechanochemical treatment. *Biomaterials* 23 **4**:1147-1152.

**Romberg, R. W., P. G. Werness, P. Lollar, B. L. Riggs, and K. G. Mann.** 1985. Isolation And Characterization Of Native Adult Osteonectin. *Journal Of Biological Chemistry* 260 **5**:2728-2736.

**Romberg, R. W., P. G. Werness, B. L. Riggs, and K. G. Mann.** 1986. Inhibition Of Hydroxyapatite Crystal-Growth By Bone-Specific And Other Calcium-Binding Proteins. *Biochemistry* 25 **5**:1176-1180.

**Ryu, O. H., A. G. Fincham, C. C. Hu, C. Zhang, Q. Qian, J. D. Bartlett, and J. P. Simmer.** 1999. Characterization of recombinant pig enamelysin activity and cleavage of recombinant pig and mouse amelogenins. *Journal Of Dental Research* 78 **3**:743-750.

**Sage, H., R. B. Vernon, S. E. Funk, E. A. Everitt, and J. Angello.** 1989. Sparc, A Secreted Protein Associated With Cellular Proliferation, Inhibits Cell

Spreading Invitro And Exhibits Ca-+2-Dependent Binding To The Extracellular-Matrix. *Journal Of Cell Biology* 109 **1**:341-356.

**Sakiyama-Elbert, S. E., and J. A. Hubbell.** 2001. Functional biomaterials: Design of novel biomaterials. *Annual Review Of Materials Research* **31**:183-201.

**Sano, K. I., H. Sasaki, and K. Shiba.** 2005. Specificity and biomineralization activities of Ti-binding peptide-1 (TBP-1). *Langmuir* 21 **7**:3090-3095.

**Sarikaya, M.** 1999. Biomimetics: Materials fabrication through biology. *Proceedings Of The National Academy Of Sciences Of The United States Of America* 96 **25**:14183-14185.

**Sarikaya, M., and I.A. Aksay**. 1995 . Biomimetics: Design and Processing of Materials . Woodbury, N.Y. : AIP Press

**Sarikaya, M., C. Tamerler, A. K. Y. Jen, K. Schulten, and F. Baneyx.** 2003. Molecular biomimetics: nanotechnology through biology. *Nature Materials* 2 **9**:577-585.

**Sarikaya, M., C. Tamerler, D. T. Schwartz, and F. O. Baneyx.** 2004. Materials assembly and formation using engineered polypeptides. *Annual Review Of Materials Research* **34**:373-408.

**Schlesinger, D. H., and D. I. Hay.** 1977. Complete Covalent Structure Of Statherin, A Tyrosine-Rich Acidic Peptide Which Inhibits Calcium-Phosphate Precipitation From Human Parotid Saliva. *Journal Of Biological Chemistry* 252 **5**:1689-1695.

**Schonbrun, J., W. J. Wedemeyer, and D. Baker**. 2002. Protein structure prediction in 2002. *Current Opinion In Structural Biology* 12 **3**:348-354.

**Schwarz, K., and M. Epple.** 1998. Biomimetic crystallization of apatite in a porous polymer matrix. *Chemistry-A European Journal* 4 **10**:1898-1903.

**Seeman, N. C., and A. M. Belcher.** 2002. Emulating biology: Building nanostructures from the bottom up. *Proceedings Of The National Academy Of Sciences Of The United States Of America* **99**:6451-6455.

**Shaw, W. J., J. R. Long, J. L. Dindot, A. A. Campbell, P. S. Stayton, and G. P. Drobny.** 2000. Determination of statherin N-terminal peptide conformation on hydroxyapatite crystals. *Journal Of The American Chemical Society* 122 **8**:1709-1716.

**Smith, G. P.** 1985. Filamentous Fusion Phage - Novel Expression Vectors That Display Cloned Antigens On The Virion Surface. *Science* 228 **4705**:1315-1317.

**Smith, G. P.**. 1988. Filamentous Phage Assembly - Morphogenetically Defective-Mutants That Do Not Kill The Host. *Virology* 167 **1**:156-165.

**Smith, G. P., and V. A. Petrenko.** 1997. Phage display. *Chemical Reviews* 97 **2**:391-410.

**Sternberg, N., and R. H. Hoess.** 1995. Display Of Peptides And Proteins On The Surface Of Bacteriophage-Lambda. *Proceedings Of The National Academy Of Sciences Of The United States Of America* 92 **5**:1609-1613.

**Tanahashi, M., T. Yao, T. Kokubo, M. Minoda, T. Miyamoto, T. Nakamura, and T. Yamamuro.** 1994. Apatite Coating On Organic Polymers By A Biomimetic Process. *Journal Of The American Ceramic Society* 77 **11**:2805-2808.

**Termine, J. D., H. K. Kleinman, S. W. Whitson, K. M. Conn, M. L. McGarvey, and G. R. Martin.** 1981. Osteonectin, A Bone-Specific Protein Linking Mineral To Collagen. *Cell* 26 **1**:99-105.

**Thotakura, S. R., T. Mah, R. Srinivasan, Y. Takagi, A. Veis, and A. George.** 2000. The non-collagenous dentin matrix proteins are involved in Dentinogenesis Imperfecta type II (DGI-II). *Journal Of Dental Research* 79 **3**:835-839.

**Veis, A.** 1993. Mineral Matrix Interactions In Bone And Dentin. *Journal Of Bone And Mineral Research* **8**:S493-S497.

**Verbeeck, R. M. H., E. A. P. Demaeyer, and F. C. M. Driessens.** 1995. Stoichiometry Of Potassium-Containing And Carbonate-Containing Apatites Synthesized By Solid-State Reactions. *Inorganic Chemistry* 34 **8**:2084-2088.

**Wang, S. Q., E. S. Humphreys, S. Y. Chung, D. F. Delduco, S. R. Lustig, H. Wang, K. N. Parker, N. W. Rizzo, S. Subramoney, Y. M. Chiang, and A. Jagota.** 2003. Peptides with selective affinity for carbon nanotubes. *Nature Materials* 2 **3**:196-200.

**Whaley, S. R., D. S. English, E. L. Hu, P. F. Barbara, and A. M. Belcher.** 2000. Selection of peptides with semiconductor binding specificity for directed nanocrystal assembly. *Nature* 405 **6787**:665-668.

**Yanagisawa, T., M. U. Nylen, and J. D. Termine.** 1981. Distribution Of Matrix Components In Hamster Enamel - An Electron-Microscopic Study. *Journal Of Dental Research* **60**:558-558.

**Zhang, H. G., Q. S. Zhu, and Y. Wang.** 2005. Morphologically controlled synthesis of hydroxyapatite with partial substitution of fluorine. *Chemistry Of Materials* 17 **23**:5824-5830.

**Zhou, H. Y., H. Takita, R. Fujisawa, M. Mizuno, and Y. Kuboki.** 1995. Stimulation By Bone Sialoprotein Of Calcification In Osteoblast-Like Mc3t3-E1 Cells. *Calcified Tissue International* 56 **5**:403-407.

**Zwick, M. B., J. Q. Shen, and J. Scott.** 1998. Phage-displayed peptide libraries. *Current Opinion In Biotechnology* 9 **4**:427-436.